NuInt02 Conference Summary: Modeling Quasi-elastic, Resonance and Inelastic Neutrino and Electron Scattering on Nucleons and Nuclei

Arie Bodek[a]

[a]Department of Physics and Astronomy, University of Rochester, Rochester, New York 14618, USA

The relationships between electron scattering and neutrino scattering on nucleons and nuclei is reviewed, aiming at better modeling of neutrino and electron scattering on nucleons and nuclei in the quasi-elastic, resonance, and inelastic regions. (Conference Summary by Arie Bodek at NuInt02, Dec. 2002, Irvine, CA, USA)

1. Introduction

Experimental evidence for oscillations among the three neutrino generations has been recently reported [1]. Present and future high intensity neutrino beams for neutrino oscillations experiments are in the 0.5-5 GeV energy region. Since quasielastic scattering(QE), resonance production, and inelastic scattering are all important components of neutrino scattering at low energies, it is important to investigate the relation between electron and neutrino scattering using the latest information on nucleon elastic, resonance production and inelastic vector and axial form factors and structure functions.

This summary is aimed at both members of the electron scattering community and members of the neutrino community. One thing to clarify is that the neutrino community uses the term 'quasielastic' to describe a charged-current process in which a neutrino interacts with a nucleon and produces a muon (or an electron) in the final state. The nucleon can be a free nucleon or a nucleon bound in the nucleus. The term 'quasielastic' refers to the fact that the initial state neutrino changes into a different lepton, and there is a single recoil nucleon in the final state (which changes its charge state). In contrast, the electron scattering community refers to the case of electron-nucleon scattering with a single recoil nucleon as 'elastic' scattering. The term 'quasielastic' scattering is used by the electron scattering community to describe elastic electron-nucleon scattering from bound nucleons in a nucleus. Here the term 'quasielastic' refers to the fact that the bound nucleon is quasi-free. Both of these interpertations are used in this article,

2. Quasielatic charged-current scattering

This topic is discussed in detail in two recent papers by Budd, Bodek and Arrington [2]. Here we give a brief summary of the results of these two papers. Recent experiments at SLAC and Jefferson Lab (JLab) have given precise measurements of the vector electromagnetic form factors for the proton and neutron. These form factors can be related to the form factors for QE neutrino scattering by conserved vector current hypothesis, CVC. These more recent form factors can be used to give better predictions for QE neutrino scattering.

The hadronic current for QE neutrino scattering is given by [3]

$$< p(p_2)|J^+_\lambda|n(p_1) >= \overline{u}(p_2)\left[\gamma_\lambda F_V^1(q^2) + \frac{i\sigma_{\lambda\nu}q^\nu\xi F_V^2(q^2)}{2M} + \gamma_\lambda\gamma_5 F_A(q^2) + \frac{q_\lambda\gamma_5 F_P(q^2)}{M}\right]u(p_1),$$

where $q = k_\nu - k_\mu$, $\xi = (\mu_p - 1) - \mu_n$, and $M = (m_p + m_n)/2$. Here, μ_p and μ_n are the proton and neutron magnetic moments. We assume that there are no second class currents, so the scalar form factor F_V^3 and the tensor form factor F_A^3 need not be included. Using the above current,

g_A	-1.267
G_F	1.1803×10^{-5} GeV^{-2}
$\cos\theta_c$	0.9740
μ_p	2.793 μ_N
μ_n	-1.913 μ_N
ξ	3.706 μ_N
M_V^2	0.71 GeV^2
M_A	1.00 GeV

Table 1
The most recent values of the parameters used in the 'BBA-2003' calculations.

the cross section is

$$\frac{d\sigma^{\nu,\ \overline{\nu}}}{dq^2} = \frac{M^2 G_F^2 cos^2\theta_c}{8\pi E_\nu^2}\times \left[A(q^2) \mp \frac{(s-u)B(q^2)}{M^2} + \frac{C(q^2)(s-u)^2}{M^4}\right],$$

where

$$A(q^2) = \frac{m^2-q^2}{4M^2}\left[\left(4-\frac{q^2}{M^2}\right)|F_A|^2 - \left(4+\frac{q^2}{M^2}\right)|F_V^1|^2 - \frac{q^2}{M^2}|\xi F_V^2|^2\left(1+\frac{q^2}{4M^2}\right) - \frac{4q^2 Re F_V^{1*}\xi F_V^2}{M^2}\right],$$

$$B(q^2) = -\frac{q^2}{M^2} Re F_A^*(F_V^1+\xi F_V^2),$$

$$C(q^2) = \frac{1}{4}\left(|F_A|^2 + |F_V^1|^2 - \frac{q^2}{M^2}\left|\frac{\xi F_V^2}{2}\right|^2\right).$$

Here

$$q^2 = q_0^2 - \vec{q}_3^2 = -4E_0E'\sin^2\frac{\theta}{2} = -Q^2\ .$$

Although we have have not shown terms of order $(m_l/M)^2$, and terms including $F_P(q^2)$ (which is multiplied by $(m_l/M)^2$), these terms are included in our calculations [3].) The form factors $F_V^1(q^2)$ and $\xi F_V^2(q^2)$ are given by:

$$F_V^1(q^2) = \frac{G_E^V(q^2) - \frac{q^2}{4M^2}G_M^V(q^2)}{1-\frac{q^2}{4M^2}},$$

$$\xi F_V^2(q^2) = \frac{G_M^V(q^2) - G_E^V(q^2)}{1-\frac{q^2}{4M^2}}.$$

We use the CVC to determine $G_E^V(q^2)$ and $G_M^V(q^2)$ from the electron scattering form factors $G_E^p(q^2)$, $G_E^n(q^2)$, $G_M^p(q^2)$, and $G_M^n(q^2)$:

$$G_E^V(q^2) = G_E^p(q^2) - G_E^n(q^2),$$
$$G_M^V(q^2) = G_M^p(q^2) - G_M^n(q^2).$$

The axial form factor F_A and the pseudoscalar form factor F_P (related to F_A by PCAC) are given by:

$$F_A(q^2) = \frac{g_A}{\left(1-\frac{q^2}{M_A^2}\right)^2},$$

$$F_P(q^2) = \frac{2M^2F_A(q^2)}{M_\pi^2-q^2}.$$

In the expression for the cross section, $F_P(q^2)$ is multiplied by $(m_l/M)^2$. Therefore, in muon neutrino interactions, this effect is very small except at very low energy, below 0.2 GeV. $F_A(q^2)$ needs to be extracted from QE neutrino scattering. At low Q^2, $F_A(q^2)$ can also be extracted from pion electroproduction data.

For later use in Adler sum rule, we express the following functions used by Adler[4] in the notation of C.H. Llewellyn Smith [3] (which we use here).

$$|F_V(q^2)|^2 = |F_V^1(q^2)|^2 - \frac{q^2}{M^2}\left|\frac{\xi F_V^2(q^2)}{2}\right|^2$$

$$g_V(q^2) = F_V^1(q^2) + \xi F_V^2(q^2)$$

Note that $F_A(q^2)$ in our notation is the same as $g_A(q^2)$ as defined by Adler, and $F_P(q^2)$ in our notation is the same as $h_A(q^2)/M$ as defined by Adler. Also, Adler defines q^2 as positive, while we define q^2 as negative and Q^2 as positive.

Previously, many neutrino experiment have assumed that the vector form factors are described by the dipole approximation.

$$G_D(q^2) = \frac{1}{\left(1-\frac{q^2}{M_V^2}\right)^2},\quad M_V^2 = 0.71\ GeV^2$$

$$G_E^p = G_D(q^2), \quad G_E^n = 0,$$
$$G_M^p = \mu_p G_D(q^2), \quad G_M^n = \mu_n G_D(q^2).$$

We refer to the above combination of form factors as 'Dipole Form Factors'. It is an approximation that has been improved by Budd, Bodek and Arington [2]. HerewWe use the updated form factors to which we refer as 'BBA-2003 Form Factors' (Budd, Bodek, Arrington). Previous neutrino experiments used g_A=−1.23, while the best current value is −1.267. The previous world average value from neutrino experiments for M_A was 1.026 ± 0.020 GeV [6]. The value of M_A extracted from neutrino experiments depends on both the value of g_A and the values of the electromagnetic form factors which are assumed in the extraction process. Here we use the updated value [2] of M_A 1.00 ± 0.020 GeV, which has been re-extracted from previous neutrino data using the better known values for g_A and the updated 'BBA-2003' vector form factors. This value of M_A is in good agreement with the theoretically corrected value from pion electroproduction [6] of 1.014 ± 0.016 GeV. Table 1 summarizes the most up to date values of the coupling constants and magnetic moments that we use in our calculations. Note that G_E^p, G_M^p, and G_E^n are positive, while G_M^n and the axial form factor F_A are negative.

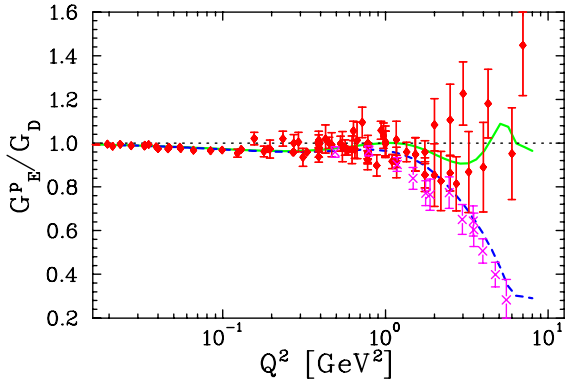

Figure 1. Fits to G_E^p/G_D, using cross section data only (solid), compared with 'BBA-2003' combined fits to both the cross section and polarization transfer data (dashed). The diamonds are the from Rosenbluth extractions and the crosses are the Hall A polarization transfer data. Note that the fit is to cross sections, rather than fitting directly to the extracted values of G_E^p shown here. Since the difference between the two is only at high Q^2, the two fits yield similar results for the predicted neutrino-nucleon cross sections.

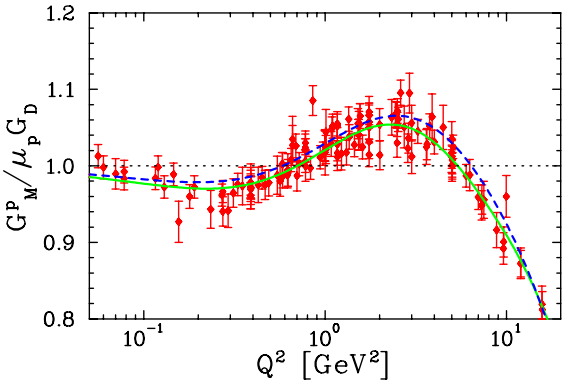

Figure 2. 'BBA-2003' fits to $G_M^p/\mu_p G_D$. The lines and symbols have the same meaning as Figure 1.

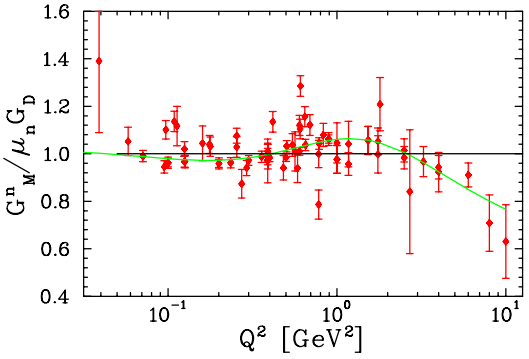

Figure 3. 'BBA-2003' fit to $G_M^n/\mu_n G_D$. The lines and symbols have the same meaning as Figure 1.

3. 'BBA-2003' updated form factors

The 'BBA-2003' updated fit to the proton electromagnetic form factors is similar to the one described in Ref. [7], but using a slightly different

	data	a_2	a_4	a_6	a_8	a_{10}	a_{12}
G_E^p	CS + Pol	3.253	1.422	0.08582	0.3318	-0.09371	0.01076
G_M^p	CS + Pol	3.104	1.428	0.1112	-0.006981	0.0003705	-0.7063E-05
G_M^n		3.043	0.8548	0.6806	-0.1287	0.008912	

Table 2
The coefficients of the inverse polynomial fits for the G_E^p, G_M^p, and G_M^n. The combined fits for the proton include both the cross section data and the Hall A polarization transfer data. Note that these different polynomials replace G_D in the expression for G_E^p, G_M^p, and G_M^n. The values in this the table along with the fit of G_E^n Krutov *et. al.* [12] (see text) will be referred to as 'BBA-2003 Vector Form Factors'.

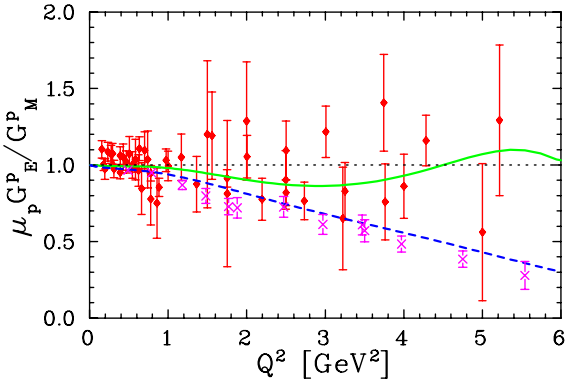

Figure 4. Ratio of G_E^p to G_M^p as extracted by Rosenbluth measurements and from polarization measurements. The lines and symbols have the same meaning as Figure 1.

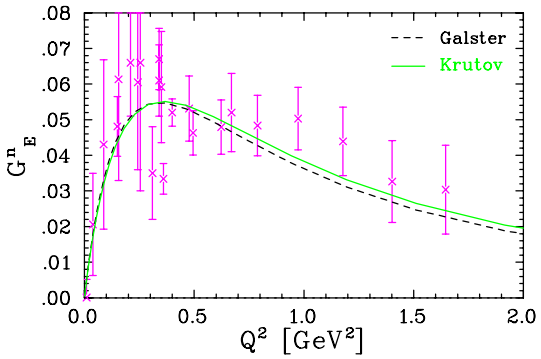

Figure 5. Data and fits to G_E^n. The dashed line is the Galster *et al.* fit [13], and the solid line is the Krutov*et al.* fit [12].

fitting function (described below), and including additional data to constrain the fit at low Q^2 values. Note that in contrast to the functional form used in Ref. [8], we only include even powers of Q in our fit. This is because odd powers of Q are not theoretically allowed. For example, one can use analyticity [9,10] to show that there are no odd terms in Q in the limit $Q \to 0$.

The vector form factors can be determined from electron scattering cross sections using the standard Rosenbluth separation technique [7], which is sensitive to radiative corrections, or from polarization measurements using the newer polarization transfer technique [11]. The polarization measurements do not directly measure the form factors, but measure the ratio G_E/G_M. Figures 1, 2, and 3 show the ratio of the fits divided by the dipole form, G_D. Figure 4 shows the 'BBA-2003' fits to $\mu_p G_E^p/G_M^p$. The fit including only cross section data is roughly flat versus Q^2 ($Q^2 = -q^2$), while ratio decreases with Q^2 in the combined fit to cross section and polarization transfer data. The combined fit to both cross section and polarization transfer data is used as the default. Although the polarization transfer measurement is believed to have smaller systematic error, especially at high Q^2, the origin of this disagreement is not known. If this disagreement comes from radiative corrections to the electron, in particular two-photon exchange terms, then the polarization transfer extraction will give the correct ratio, but the overall scale of G_E^p at low Q^2 would be shifted down by ≈3%. Because the fit is constrained as $Q^2 \to 0$, there will not be an overall shift in G_E^p at low Q^2, but there will be some uncertainty in the low Q^2 behavior. Current experiments at JLab aim to better understand the source of the disagreement by

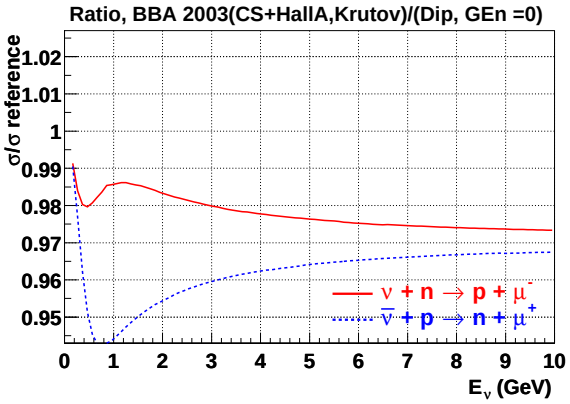

Figure 6. Ratio versus energy of predicted neutrino (antineutrino) QE cross section using BBA-2003 Form Factors to the prediction using the dipole approximation with G_E^n=0 (with M_A kept fixed).

looking at the recoil proton in elastic electron-proton scattering, thus minimizing the sensitivity to the dominant sources of uncertainty in previous Rosenbluth separations. However, since this discrepancy is most prominent at high Q^2, and the fit is constrained at low Q^2, it has only a relatively small effect on the neutrino QE scattering cross section.

To account for the fact that deviations from the dipole form are different for each of the different form factors, the electron scattering data are fit for each of the form factors to an inverse polynomial

$$G_{E,M}^N(Q^2) = \frac{G_{E,M}^N(Q^2=0)}{1 + a_2 Q^2 + a_4 Q^4 + a_6 Q^6 + \ldots}.$$

Table 2 shows the parameters of the 'BBA-2003' fit to the proton data using both cross section data together with the polarization transfer data from JLab Hall A. For G_E^p, the parameters in Table 2 are used for $Q^2 < 6$ GeV^2. For $Q^2 > 6$ GeV^2, the ratio of G_E^p/G_M^p is assumed to be constant:

$$G_E^p(Q^2) = G_M^p(Q^2)\frac{G_E^p(6\text{ GeV}^2)}{G_M^p(6\text{ GeV}^2)}$$

Since the neutron has no charge, G_E^n must be zero at q^2=0, and previous neutrino experiments assumed $G_E^n(q^2)$=0 for all q^2 values. However, it is non-zero away from q^2=0, and its slope at q^2=0 is known precisely from neutron-electron scattering. At intermediate Q^2, recent polarization transfer data give precise values of $G_E^n(q^2)$. Our analysis uses the parameterization of Krutov *et. al.* [12]:

$$G_E^n(Q^2) = -\mu_n \frac{a\tau}{1+b\tau} G_D(Q^2), \quad \tau = \frac{Q^2}{4M^2},$$

with $a = 0.942$ and $b = 4.61$. This parameterization is very similar to that of Galster *et al.* [13], as shown in Figure 5. The parameters in Table 2, along with the fit of G_E^n of Krutov *et. al.* [12], are referred to as 'BBA-2003 Form Factors'. For BBA-2003 Form Factors, both the cross section and polarization data are used in the extraction of G_E^p and G_M^p.

Figure 6 shows the ratio versus neutrino energy of the predicted neutrino (antineutrino) QE cross section on nucleons using the 'BBA-2003' Vector Form Factors to the prediction using the Dipole Vector Form Factors (with G_E^n=0 and M_A kept fixed). This plot indicates that it is important to use the updated form factors.

4. A re-extraction of the axial form factor

Previous neutrino measurements, mostly bubble chamber experiments on deuterium, extracted M_A using the best known assumptions at the time. Changing these assumptions changes the extracted value of M_A. Hence, M_A needs to be updated using new form factors and up-to-date couplings. Budd, Bodek and Arrington updated the results from three previous deuterium bubble chamber experiments. These are Baker *et al.* [14], Barish *et al.* [15], Miller *et al.* [16], and Kitagaki *et al.* [17]. Barish *et al.* and Miller *et al.* are the same experiment, with the analysis of Miller *et al.* including the full data set, roughly three times the statistics included in the original analysis. On average, correcting for the various assumptions in form factors and couplings results in a decrease of 0.026 in the extracted value of M_A. This is why we use a value of 1.00 instead of the previous world average of 1.026. Figure 7 shows the Q^2 distribution from the Baker *et al.* [14] neutrino

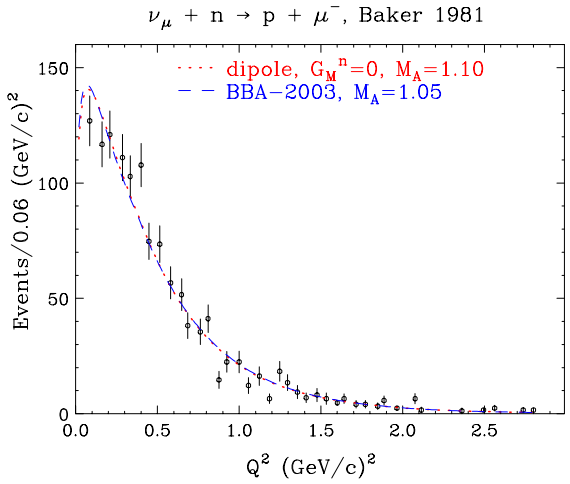

Figure 7. A comparison of the Q^2 distribution using 2 different sets of form factors. The data are from Baker *et al.* [14]. The dotted curve uses Dipole Form Factors with $G_E^n = 0$ and $M_A = 1.10\ GeV$. The dashed curve uses BBA-2003 Form Factors with $M_A = 1.05\ GeV$. The two curves cannot be distinguished from one another. This illustrates that it is important to use the most up to date information on vector form factors from electron scattering experiments when extracting the axial form factor from neutrino data.

experiment compared to the prediction assuming Dipole Form Factors with G_E^n=0 and M_A=1.10 GeV. Also shown are the prediction using BBA-2003 Form Factors and M_A=1.050 GeV. When we modify the electromagnetic form factors, we can use a diffeernt M_A to describe the same Q^2 distribution. Although the overall total cross sections are different, there is no modification of the Q^2 dependence when a contribution to the distribution is shifted between the electromagnetic and axial form factors. Therefore, we conclude that with the same value of g_A, the use of Dipole Form Factors (and Gen =0) instead of the BBA-2003 form factors lead to an error in extracted value of M_A of 0.050 GeV, independent of the details of the experiment.

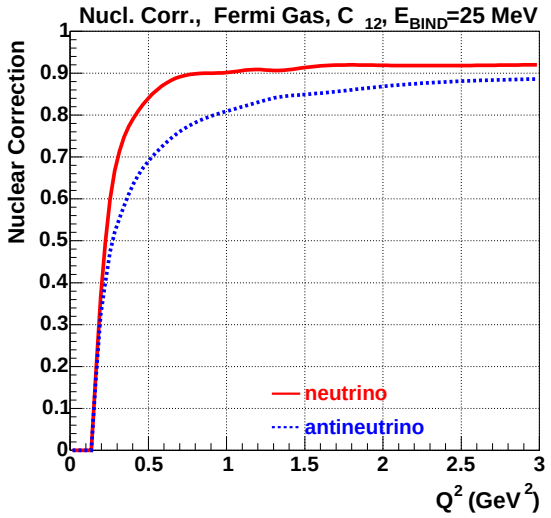

Figure 8. (a) The Pauli blocking suppression for a Fermi gas model for carbon with a 25 MeV binding energy and 220 MeV Fermi momentum.

5. Nuclear Effects in Quasielastic Scattering from Bound Nucelons

There are three important effects on the inclusive quasielastic cross section on nuclear targets. These are (a) Fermi Motion, (b) Pauli Blocking and (c) Binding corrections to the nucleon form factors due to distortion of the both the nucleon size or distortions of the pion cloud around the nucleon in the nucleus. Figure 8 shows the nuclear suppression versus Q^2 from a NUANCE [32] calculation [29] of a Smith and Moniz [30] based Fermi gas model for carbon. This nuclear model includes Pauli blocking and Fermi motion (but not final state interactions). The Fermi gas model was run with a 25 MeV nuclear potential binding energy ϵ and 220 MeV Fermi momentum K_f. Figure 9 from Moniz et. al. [30] shows how the effective K_f and nuclear potential binding energy ϵ (within a Fermi-gas model) for various nuclei was extracted from electron scattering data. The effective K_f is extracted from the width of the

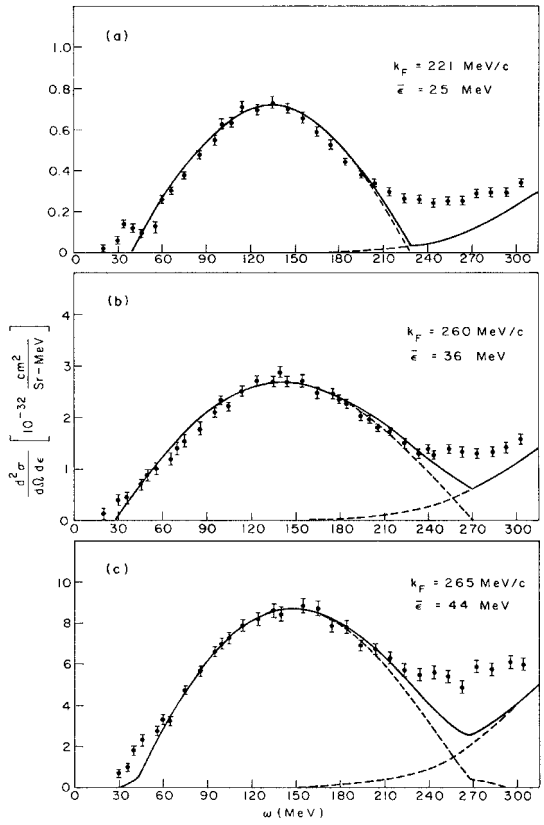

Figure 9. Extraction of the Fermi Gas model parameters i.e. the effective K_f and nuclear potential binding energy ϵ from 500 MeV electron scattering data (from Moniz. [30]. (a)Carbon, (b) Nickel and (c) Lead

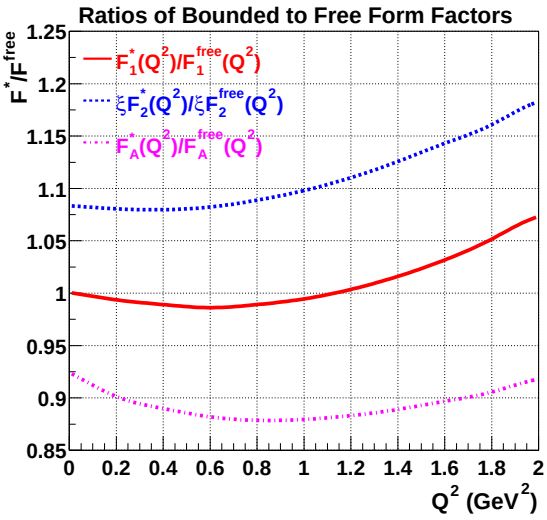

Figure 10. The ratio of bound nucleon (in Carbon) to free nucleon form factors for F_1, F_2, and F_A from ref [33]. Note that this model is only relevant for Q^2 less than 1 GeV^2, and that the binding effects on the form factors are expected to be very small at higher Q^2. At low Q^2 the effect of the nuclear binding effects from this model are similar to what is observed in experiments at Jlab [35].

electron scattered energy, and the nuclear potential binding energy ϵ is extracted from the shifted location of the quasielastic peak. Figure 12 shows the effective K_f for various nuclear targets.

Figures 10 and 11 show the prediction for the nuclear binding effect on the nucleon form factors (i.e. the ratio of bound to free nucleon form factors for F_1, F_2, F_A) in neutrino scattering, and for the vector form factors G_E^p, G_E^n, G_M^p and G_M^n in electron scattering as modeled by Tsushima *et al* [33]. Note that this model is only relevant for Q^2 less than 1 GeV^2, and that experiments from Jlab indicate that the binding effects on the form factors are expected to be very small at higher Q^2 (see next section).

At low Q^2 the effect of the nuclear binding effects from this model are similar to what is observed in experiments at Jlab [35]. Both the Pauli blocking and the nuclear modifications to bound nucleon form factors reduce the cross section relative to the cross section with free nucleons.

6. Detection of recoil nucleons

The calculation for the inclusive cross section assumes that only the final state muon is detected. In neutrino experiments, detection of

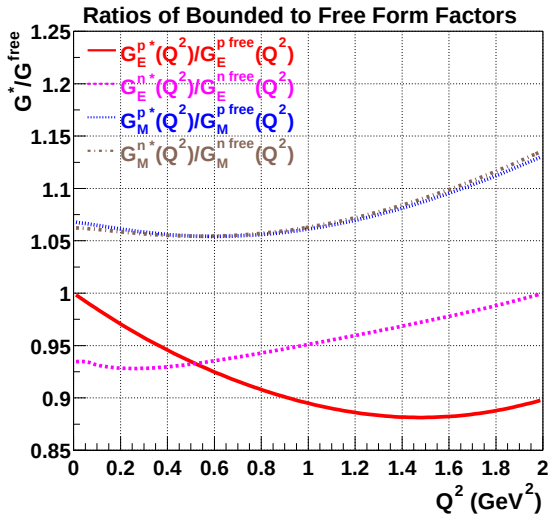

Figure 11. The ratio of bound nucleon (in Carbon) to free nucleon form factors for G_E^p, G_E^n, G_M^p and G_M^n from ref [33]. Note that this model is only relevant for Q^2 less than 1 GeV^2, and that the binding effects on the form factors are expected to be very small at higher Q^2. At low Q^2 the effect of the nuclear binding effects from this model are similar to what is observed in experiments at Jlab [35].

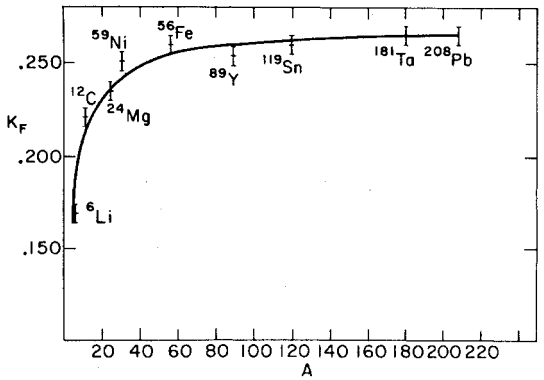

Figure 12. Fits to the effective K_f (within a Fermi-gas model) for various nuclei from Moniz. [30] used by Bodek and Ritchie.

the recoil nucleon is sometimes required in order to differentiate between quasielastic and inelastic events. Therefore, the final state interaction of the final state proton with the remaining nucleons also needs to be modeled (which leads to a reduction of the number of identified quasielastic events). Similarly, quasielastic scattering with nucleons in the high momenta region of the spectral functions also needs to be modeled. This requires more sophisticated models than the simple Fermi-Gas model. Conversely, inelastic events (such as in resonance production) may be misidentified as quasielastic events if the final state pion is absorbed in the nucleus. The best way to model these effects is to do an analysis on samples of electron scattering data on nuclear targets (including the hadronic final states) in order to test the effects of the experimental cuts on the final state nucleons. This kind of study is being planned by a Rochester group [36] in collaboration with the Hall B CLAS collaboration. Such an investigation also tests the validity of the binding off-shell corrections to the nucleon form factors for nucleons bound in a nucleus.

Current e,e'p experiments at intermediate Q^2 are not well described by the impulse approximation with distortion effects. One is forced to introduce a quenching factor which is large for low $Q^2 \sim 0.3$ GeV^2. This effect has been modeled by Tsushima *et al* [33] as binding corrections to nucleon form factors. However this factor cannot be strickly interpreted as a change of the form factor of the nucleus because for large Q^2 the suppression becomes much smaller and may be practically gone [35] by Q^2=2 GeV^2.

The interpertation of M. Strikman and others [35] is that one is dealing here with renormalization of the interaction of nucleons at low energy scale (natural in the Fermi liquid theory) which is essentially gone at large Q^2. What this implies for low Q^2 is basically the statement that the theory is not good enough and hence it is difficult to calculate cross section in νA scattering

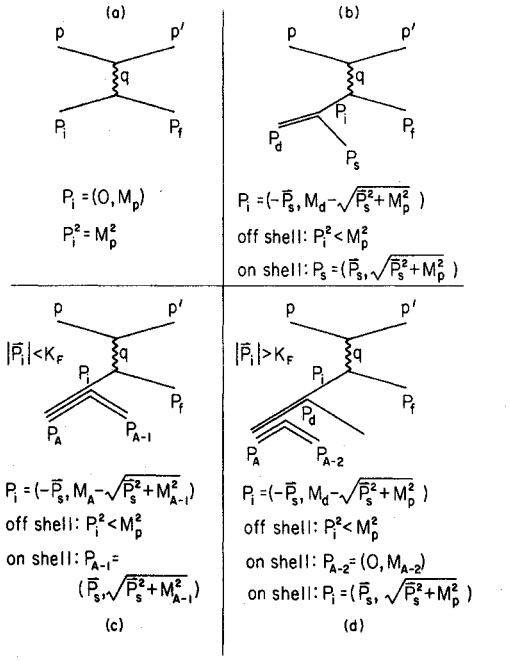

Figure 13. Kinematics for on-shell and off-shell scattering and scattering from off-shell nucleons in deuterium and nuclei. (a) Free nucleons. (b) A nucleon bound in the deuteron. (c) A nucleon with momentum $|\vec{P}_i| < K_F$ in a heavy nucleus of atomic weight A. (d) A nucleon bound in a heavy nucleus having momentum $|\vec{P}| > K_F$ due to an interaction with another nucleon. See text for details.

at low Q^2 from first principles. It is not clear how well the rescaling from e,e' to νA will work under these conditions. There may be some differences since the pion field plays a rather different rols in two cases (as can be seen from the different masses entering in the axial and vector electromagnetic form factors). Therefore, one should take the predictions of the model of Tsushima *et al* [33] only as an indication of the possible magnitude of these effects (and use it only at low Q^2). More theoretical and experimental studies are needed. As discussed in a later section, the MiniBoone and JPARC experiments can help address this question by investigating nuclear and binding effects in Carbon in neutrino scattering, and compare the data to nuclear effects observed in electron scattering at Jlab.

7. Plane Wave Impulse Approximation (PWIA)

A. Free protons

Here we describe an treatment of Bodek and Ritchie, and also add the effect of the nuclear binding potential ϵ as described in Moniz. [30]. Before we discuss the kinematics of the scattering from an off-shell nucleon in a deuterium or heavy target nucleus, we consider the case of scattering from a free proton. We take the case of electron scattering to represent the general lepton-nucleon scattering at high energies. The kinematics of the scattering from a free proton of mass M_p is shown in Figure 13(a). The incident electron energy is E_0 and the final scattering energy in the laboratory system is E'. The scattering angle in the laboratory is defined as θ. The four-momentum transfer to the target proton is $q = (\vec{q}_3, q_0)$. We define the following variables in terms of laboratory energies and angles. The square of the invariant four-momentum transfer q is

$$q^2 = q_0^2 - \vec{q}_3^2 = -4E_0E'\sin^2\frac{\theta}{2} = -Q^2 \ .$$

The square of the initial target proton four-momentum P_i is

$$P_i^2 = M_p^2 \ .$$

The square of the final-state proton momentum P_f (which is equal to the final-state invariant mass) is

$$\begin{aligned} P_f^2 &= W^2 = (P_i + q)^2 = P_i^2 + 2P_i \cdot q + q^2 \\ &= M_p^2 + 2M\nu - Q^2 \ , \end{aligned}$$

where $\nu = E_0 - E' = q_0$ (in the laboratory system) and $x = Q^2/2q \cdot P_i = Q^2/2M_p\nu$.

B. Scattering from an off-shell nucleon in the deuteron

In the impulse approximation, the spectator nucleon in the deuteron is free and is on the mass

shell. It is totally unaffected by the interaction. The interacting nucleon with momentum P_i must be of the mass shell in order to conserve energy and momentum in the scattering process. The kinematics is shown in Figure 13(b). The Fermi motion does not change Q^2 but it does change the final-state invariant mass W and the quantity $P_i \cdot q$. Because the interacting nucleon is off the mass shell, its effective mass is less than the mass of the proton and is a function of its momentum. The on-shell spectator has momentum $\vec{P}_s$ and on-shell energy $E_s = (\vec{P}_s^2 + M_p^2)^{1/2}$. The off-shell interacting proton has momentum $-\vec{P}_s$ and off-shell energy in the laboratory $E_i = M_d - E_s$, where M_d is the mass of the deuteron, i.e.,

$$\vec{P} = \vec{P}_i = -\vec{P}_s \quad \text{and} \quad E_i = M_d - (P_s^2 + M_p^2)^{1/2} \ .$$

After the scattering the invariant mass of the final state (neglecting the free spectator) is

$$\begin{aligned} P_f^2 &= W'^2 = (P_i + q)^2 = P_i^2 + 2P_i \cdot q - Q^2 \ , \\ W'^2 &= (E_i^2 - \vec{P}_s^2) + 2E_i\nu - 2P_3|\vec{q}_3| - Q^2 \ , \end{aligned}$$

where P_3 is the momentum along the direction of the $\vec{q}_3$ vector.

C. Scattering from an off-shell nucleon in the nucleus ($P < K_F$)

For momenta less than the Fermi momenta K_F, the nucleon interacts with the average potential of all the nucleons in the nucleus of atomic weight A. Therefore, in the impulse approximation, the interacting nucleon has momentum P_i which is balanced by a excited recoiling nucleus with $A-1$ nucleons and momentum $P_{A-1} = -P_i$. The interacting nucleon is off the mass shell, and the recoiling excited $A-1$ nucleus is on the mass shell. After the collision, the recoiling nucleus remains in its excited state, M^*_{A-1} and all the particles are on the mass shell [see Figure 13(c)]. In the laboratory system we have

$$\vec{P} = \vec{P}_i = -\vec{P}_s, \quad E_i = (\vec{P}^2 + M_p^2)^{1/2} - \epsilon \ ,$$

where ϵ is the effective depth of average nucleon potential energy in GeV (e.g. 25 MeV for Carbon) and

$$W'^2 = (E_i^2 - \vec{P}_2^2) + 2E_i\nu - 2P_3|\vec{q}| - q^2 \ .$$

This process leaves behind an $A-1$ nucleus in an excited state M^*_{A-1}, which does not need to be calculated, but varies with $\vec{P}$ such that the following equation also holds

$$(\vec{P}_s^2 + M^{*2}_{A-1})^{1/2} = M_A - E_i \ ,$$

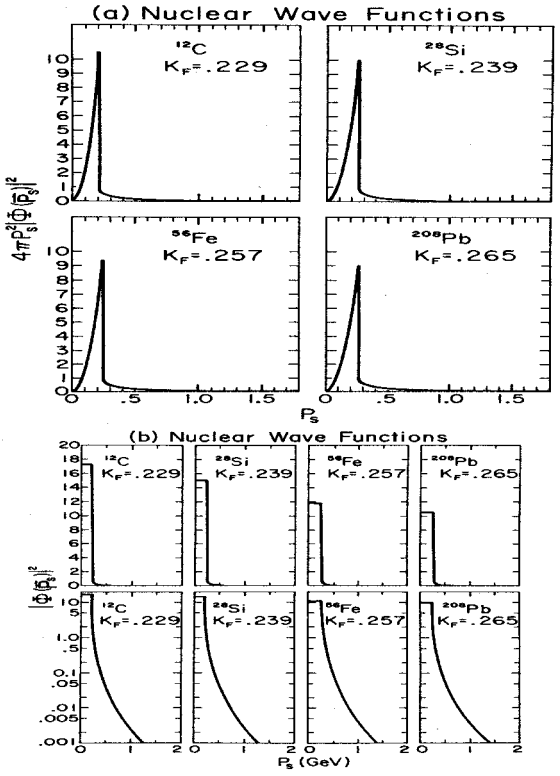

Figure 14. Fermi Gas wave functions, with and without a quasideuton tail. These momentum distributions used in the calculations of Bodek and Ritchie for ^{12}C, ^{28}Si,^{56}Fe and ^{208}Pb. (a) $4\pi|\vec{P}|^2\phi(\vec{P})|^2$. (b) $|\phi(\vec{P})|^2$

D. Scattering from an off-shell nucleon in the nucleus ($P \gg K_F$)

In the simple Fermi-gas model the nucleons cannot have momenta greater than the Fermi momentum K_F. However, such high momenta can

come from the interaction between individual nucleons through their hard-core potential. In the case where the nucleon has acquired its high momentum by interacting with another single nucleon, one may assume that a single nucleon is recoiling against it. This case can be treated as having a quasideuteron in the nucleus with a excited spectator nucleus of $A-2$ nucleons which is at rest in the laboratory system. If we neglect the excitation energy of the spectator nucleus, the kinematics [shown in Figure 13(d)] are the same as the scattering from a nucleon bound in the deuteron. However (within this rather simplified model for the high mometum tails) one can also correct for the fact that the $A-2$ nucleons are on average in an excited state because two nucleons each with average binding potential energy ϵ were removed:

$$\vec{P} = \vec{P}_i = -\vec{P}_s \quad \text{and} \quad E_i = M_d - (P_s^2 + M_p^2)^{1/2} - 2\epsilon \ .$$

E. Nuclear Momentum Distributions

If the Fermi-Gas model is to used to predict neutrino cross sections on nuclei, it is best to use Fermi-gas momentum distributions that are obtained from fits to quasielastic electron-scattering data from heavy nuclei. In the Fermi-gas model the momentum distribution is constant up to the maximum Fermi momentum K_F and is zero above K_F. One can also add a high-momentum tail to the momentum distribution (according to Moniz [31]) which is based on calculations of nucleon-nucleon correlations in nuclear matter. The normalized momentum distributions with tail (e.g. if we use this model up to P_{max}= 0.75 GeV) are:

$$|\phi(\vec{P})|^2 = \frac{1}{C}\left[1 - 6\left(\frac{K_F a}{\pi}\right)^2\right]$$

$$\text{for } 0 < |\vec{P}| < K_F \ ,$$

$$|\phi(\vec{P})|^2 = \frac{1}{C}\left[2R\left(\frac{K_F a}{\pi}\right)^2\left(\frac{K_F}{P}\right)^4\right]$$

$$\text{for } K_F < |\vec{P}| < P_{max} \ ,$$

$$|\phi(\vec{P})|^2 = 0 \text{ for } |\vec{P}| > P_{max}$$

with $a = 2$ (GeV/c)$^{-1}$, $C = \frac{4}{3}\pi K_F^3$, and $R = 1/[1 - K_F/(P_{max}]$. These momentum distributions satisfy the normalization

$$\int_0^{P_{max}} |\phi(\vec{P})|^2 4\pi P^2 dp = 1.0 \ .$$

The difference in the momentum distributions for protons and neutrons is taken into account as follows:

$$K_F^p = K_F\left(\frac{2Z}{A}\right)^{1/3} \ ,$$

$$K_F^n = K_F\left(\frac{2N}{A}\right)^{1/3} \ ,$$

where $A = A + N$ is the atomic weight. Z is the number of protons, and N is the number of neutrons. For an isoscalar target $Z = N = A/2$ and $K_F^p = K_F^n = K_F$. The momentum distribution for carbon (^{12}C), silicon (^{28}Si), iron (^{56}Fe), and lead (^{208}Pb) are shown in linear and logarithmic scales in Figures 14(b) and 13(a). The Fermi momenta that are shown are 0.221 GeV/c for ^{12}C, 0.257 GeV/c for ^{56}Fe, and 0.265 GeV/c for ^{208}Pb. These are from fits by Moniz, which also extracted ϵ values of 25, 36 and 44 MeV, respectively.

Although in the original paper of Bodek and Ritchie the form for the additional tail was used up to momenta of P_{max}=4 GeV/c, it is probably better to use this tail only up to P_{max}=0.75 GeV/c. For a calculation which does not include the additional tail, the expressions are:

$$|\phi(\vec{P})|^2 = \frac{1}{C} \text{ for } 0 < |\vec{P}| < K_F \ ,$$

$$|\phi(\vec{P})|^2 = 0 \text{ for } |\vec{P}| > K_F$$

F. Nuclear Spectral functions

The above Fermi Motion model, with or without tail is relatively easy to use in Monte Carlo simulations. The Fermi gas model is a special case of a spectral function with specific approximation to the momentum distribution and nucleon removal energy. More refined models use electron scattering data to extract spectral functions which give the correlated information between the momentum of the nucleon and the nucleon removal potential binding for the different

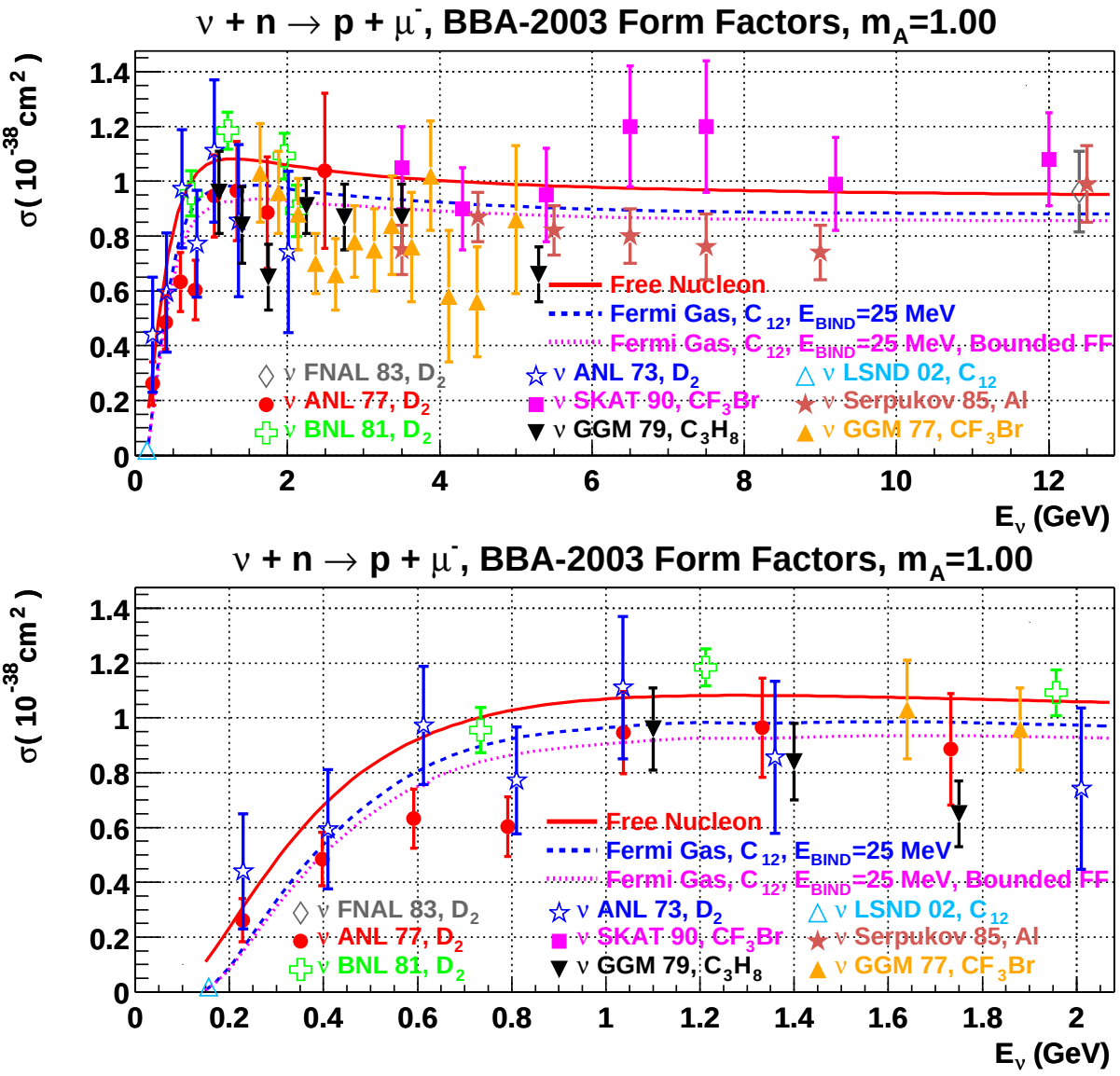

Figure 15. The QE neutrino cross section along with data from various experiments. The calculation uses M_A=1.00 GeV, g_A=−1.267, M_V^2=0.71 GeV^2 and BBA-2003 Form Factors. The solid curve uses no nuclear correction, while the dashed curve [29] uses a Fermi gas model for carbon with a 25 MeV binding energy and 220 Fermi momentum. The dotted curve is the prediction for Carbon including both Fermi gas Pauli blocking and the effect of nuclear binding on the nucleon form factors [33]. The lower plot is identical to the upper plot with the E_ν axis limit changed to 2 GeV. The data shown are from FNAL 1983 [17], ANL 1977 [15], BNL 1981 [14], ANL 1973 [22], SKAT 1990 [23], GGM 1979 [24], LSND 2002 [25], Serpukov 1985 [26], and GGM 1977 [27].

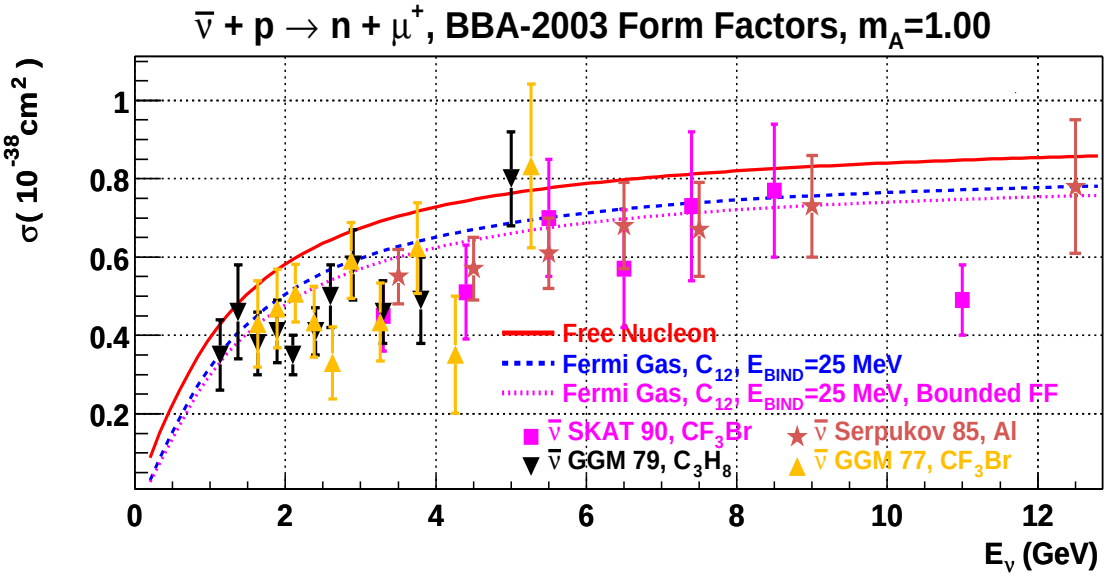

Figure 16. The QE antineutrino cross section along with data from various experiments. The calculation uses M_A=1.00 GeV, g_A=−1.267, M_V^2=0.71 GeV^2 and BBA-2003 Form Factors. The solid curve uses no nuclear correction, while the dashed curve [29] uses a Fermi gas model for carbon with a 25 MeV binding energy and 220 MeV Fermi momentum. The dotted curve is the prediction for Carbon including both Fermi gas Pauli blocking and the effect of nuclear binding on the nucleon form factors [33]. The data shown are from SKAT 1990 [23], GGM 1979 [28], Serpukov 1985 [26], and GGM 1977 [27].

shell-model nucleons in different energy levels in the nucleus.

However, it is important to realize that as long as the parameters within a given nuclear model are empirically fit and extracted from electron scattering data, these models can be used rather reliably to predict the corresponding nuclear effects in neutrino scattering (especially for vector scattering).

8. Future extractions of the axial form factor

Current and future high statistics neutrino experiments at low energies (such as MiniBoone, JPARC and MINERvA) use an active nuclear target such as scintillator (e.g. Carbon). The maximum Q^2 values that can be reached with neutrino energies of 0.5, 1.0, 1.5 and 2 GeV are 0.5, 1.2, 2,1 and 2.9 GeV^2. Since MiniBoone and JPARC energies are in the 0.7 GeV range, these experiments probes the low $Q^2 < 1\ GeV^2$ region where nuclear effects are very large (see Figures 8 and 10) and where the axial from factor is already known very well from neutrino data on deuterium (see Figure 7). The low Q^2 ($Q^2 < 1\ GeV^2$) MiniBoone and JPARC experiments can investigate the various nuclear and binding effects in Carbon in neutrino scattering versus those observed in electron scattering at Jlab.

At higher Q^2 GeV^2, as shown by the BBA-2003 fits to the vector form factors, the dipole approximation can be as much as factor of 2 wrong for the vector form factors for $Q^2 > 2GeV^2$. Therefore, there is no reason for this form to also be valid for the axial form factors. As can be seen from Figure 7 there is very little data for the axial form factor in the high Q^2 region (where nuclear effects are smaller). Both the low Q^2 ($Q^2 < 1\ GeV^2$) and

high Q^2 ($Q^2 > 2\ GeV^2$) regions are accessible at higher energy experiments such as MINERvA [37] at Fermilab (which can span the 2-8 GeV energy neutrino range).

Note that the high Q^2 region does not contribute much to the total quasielastic cross section. Therefore, it does not contribute much to the uncertainties in the total cross section. The measurement of the axial form factor in the high Q^2 region (which can be done in MINERvA) is mostly of interest in the investigation of the vector and axial structure of the nucleon.

9. Comparison to Experimental Data

Figures 15, and 16 show the QE cross section for ν and $\overline{\nu}$ with BBA-2003 Form Factors and M_A=1.00 GeV. The normalization uncertainty in the data is approximately 10%. The solid curve uses no nuclear correction, while the dashed curve [29] uses a NUANCE [32] calculation of a Smith and Moniz [30] based Fermi gas model for carbon. This nuclear model includes Pauli blocking (see Figure 8). The dotted curve is the prediction for Carbon including both Fermi gas Pauli blocking, and the effect of nuclear binding on the nucleon form factors as modeled by Tsushima *et al* [33] (see Figure 10).

The updated form factors improve the agreement with neutrino QE cross section data and give a reasonable description of the cross sections from deuterium.

Bodek, Budd and Arrington plan to continue to study the nuclear corrections, adopting models which have been used in precision electron scattering measurements from nuclei at SLAC and JLab. For example, investigation of the Pauli blocking correction using an improved Fermi Gas model with a high momentum tail [34], and more sophisticated nuclear spectral functions. In addition, the the extraction of M_A from previous neutrino experiments, using the updated versions of the input parameters and electromagnetic form factors is continuing.

10. Inelastic Scattering: Origin of Higher Twist Terms

The quark distributions in the proton and neutron are parametrized as Parton Distribution Functions (PDFs) obtained from global fits to various sets of data at very high energies. These fits are done within the theory of Quantum Chromodynamics (QCD) in either leading order (LO) or next to leading order (NLO). The most important data come from deep-inelastic e/μ scattering experiments on hydrogen and deuterium, and ν_μ and $\overline{\nu}_\mu$ experiments on nuclear targets. In previous publications [42–44] Bodek and Yang have compared the predictions of the NLO MRSR2 PDFs to deep-inelastic e/μ scattering data [45] on hydrogen and deuterium from SLAC, BCDMS and NMC. In order to get agreement with the lower energy SLAC data for F_2 and R down to Q^2=1 GeV^2, and at the highest values of x ($x = 0.9$), Bodek and Yang found that the following modifications to the NLO MRSR2 PDFs must be included.

1. The relative normalizations between the various data sets and the BCDMS systematic error shift must be included [42,43].

2. Deuteron binding corrections need to be applied and the ratio of d/u at high x must be increased as discussed in ref. [42].

3. Kinematic higher-twist originating from target mass effects [46] are very large and must be included.

4. Dynamical higher-twist corrections are smaller but also need to be included [42,43].

5. In addition, the analysis including QCD Next to NLO (NNLO) terms shows [43] that most of the dynamical higher-twist corrections needed to fit the data within a NLO QCD analysis originate from the *missing NNLO higher order terms*.

The Bodek-Yang analysis shows that the NLO MRSR2 PDFs with target mass and NNLO higher order terms describe electron and muon scattering F_2 and R data with a very small contribution from higher twists. Figures 17 shows

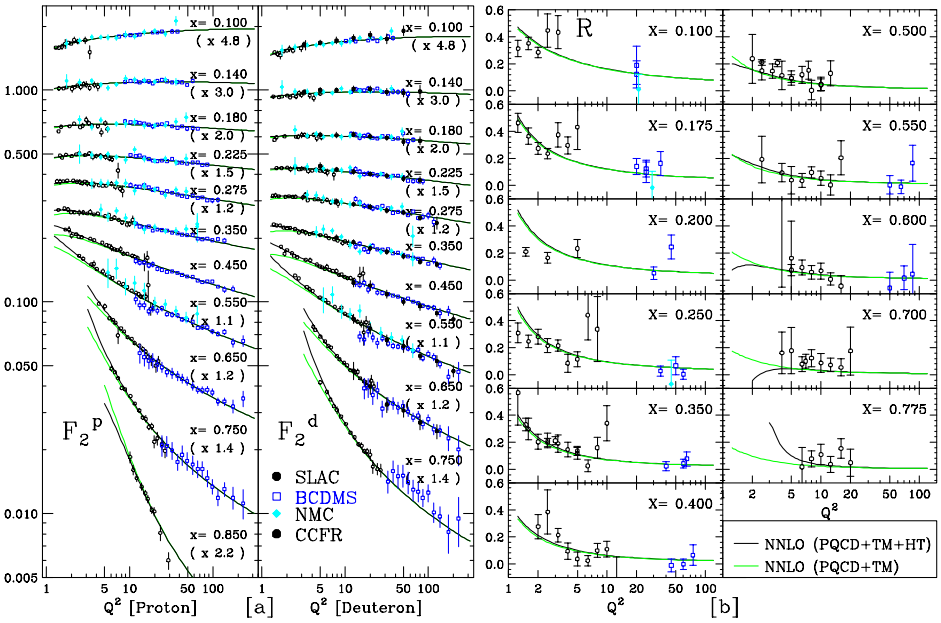

Figure 17. Electron and muon data (SLAC, BCDMS and NMC) for F_{2p} [a] and R [b] compared to the predictions with MRSR2 NLO PDFs including both NNLO and target mass corrections with (solid line) and without (dashed line) higher twist corrections (From Yang and Bodek Ref. [43]). These studies indicate that in QCD LO or NLO fits, the extracted higher twist corrections originate from target mass effects and the missing QCD NNLO higher order terms (for $Q^2 > 1$ GeV^2).

that the NLO MRSR2 PDFs with target mass and NNLO higher order terms describe electron and muon scattering F_2 and R data with a very small contribution from higher twists. Studies by other authors [47] also show that in NNLO analyses the dynamic higher twist corrections are very small. If (for $Q^2 > 1$ GeV^2) most of the higher-twist terms needed to obtain agreement with the low energy data actually originate from target mass effects and missing NNLO terms (i.e. not from interactions with spectator quarks) then these terms should be the same in ν_μ and e/μ scattering. Therefore, low energy ν_μ data should be described by the PDFs which are fit to high energy data and are modified to include target mass and higher-twist corrections that fit low energy e/μ scattering data. However, for $Q^2 < 1$ GeV^2 additional non-perturbative effects from spectator quarks must also be included [48].

11. Previous Results with GRV94 PDFs and x_w

Initially [48], Bodek and Yang used a modified scaling variable x_w and fit for modifications to the GRV94 leading order PDFs such that the PDFs describe both high energy and low energy e/μ data. In order to describe low energy data down to the photoproduction limit ($Q^2 = 0$), and account for both target mass and higher twist effects, the following modifications of the GRV94 LO PDFs are need:

1. Increased the d/u ratio at high x as described in ref. [42].

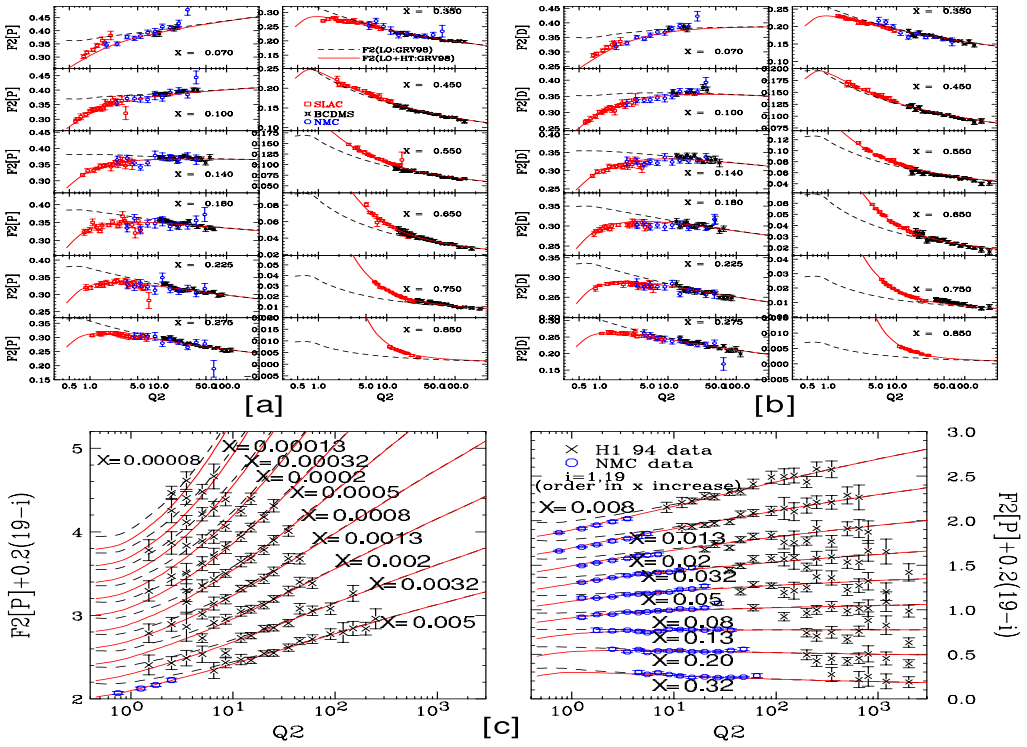

Figure 18. Electron and muon F_2 data (SLAC, BCDMS, NMC, H1 94) used in our GRV98 ξ_w fit compared to the predictions of the unmodified GRV98 PDFs (LO, dashed line) and the modified GRV98 PDFs fits (LO+HT, solid line); [a] for F_2 proton, [b] for F_2 deuteron, and [c] for the H1 and NMC proton data at low x.

2. Instead of the scaling variable x use the scaling variable $x_w = (Q^2 + B)/(2M\nu + A)$ (or $= x(Q^2 + B)/(Q^2 + Ax)$). This modification was used in early fits to SLAC data [50]. The parameter A provides for an approximate way to include *both* target mass and higher twist effects at high x, and the parameter B allows the fit to be used all the way down to the photoproduction limit (Q^2=0).

3. In addition as was done in earlier non-QCD based fits [51] to low energy data, multipliy all PDFs by a factor K=Q^2 / (Q^2 +C). This was done in order for the fits to describe low Q^2 data in the photoproduction limit, where F_2 is related to the photoproduction cross section according to

$$\sigma(\gamma p) = \frac{4\pi^2 \alpha_{\rm EM}}{Q^2} F_2 = \frac{0.112 mb\ GeV^2}{Q^2} F_2$$

4. Finally, the evolution of the GRV94 PDFs is frozen at a value of $Q^2 = 0.24$ (for $Q^2 < 0.24$), because GRV94 PDFs are only valid down to $Q^2 = 0.23$ GeV^2.

In the analysis, the measured structure functions were corrected for the BCDMS systematic error shift and for the relative normalizations between the SLAC, BCDMS and NMC data [42,43]. The deuterium data were corrected

for nuclear binding effects [42,43]. A simultaneous fit to both proton and deuteron SLAC, NMC and BCDMS data (with $x > 0.07$ only) yields A=1.735, B=0.624 and C=0.188 (GeV^2) with GRV94 LO PDFs (χ^2 = 1351/958 DOF). Note that for x_w the parameter A accounts for *both* target mass and higher twist effects.

12. New Analysis of Bodek-Yang with ξ_w, G_D and GRV98 PDFs

The initial study has been updated [49] using a new improved scaling variable ξ_w, and the fit done for modifications to the more modern GRV98 LO PDFs such that the PDFs describe both high energy and low energy electron/muon data. In addition NMC and H1 94 data at lower x are added. The the evolution of the GRV98 PDFs is frozen at a value of $Q^2 = 0.8$ (for $Q^2 < 0.8$), because GRV98 PDFs are only valid down to $Q^2 = 0.8$ GeV^2. In addition, different photoproduction limit multiplicative factors are used for valence and sea. The proposed new scaling variable is based on the following derivation. Using energy momentum conservation, it can be shown that the factional momentum $\xi = (p_z + p_0)/(P_z + P_0)$ carried by a quark of 4-mometum p in a proton target of mass M and 4-momentum P is given by $\xi = xQ^{'2}/[0.5Q^2(1+[1+(2Mx)^2/Q^2]^{1/2})]$, where $2Q^{'2} = [Q^2+{M_f}^2-{M_i}^2]+[(Q^2+{M_f}^2-{M_i}^2)^2+4Q^2({M_i}^2+P_T^2)]^{1/2}$.

Here M_i is the initial quark mass with average initial transverse momentum P_T and M_f is the mass of the quark in the final state. The above expression for ξ was previously derived [46] for the case of $P_T = 0$. Assuming $M_i = 0$ we use instead:

$\xi_w = x(Q^2 + B + {M_f}^2)/(0.5Q^2(1 + [1 + (2Mx)^2/Q^2]^{1/2}) + Ax)$

Here M_f=0, except for charm-production processes in neutrino scattering for which M_f=1.3 GeV (in leading order).(Note that this is an effective charm quark mass which is extracted from leading order fits to neutrino production of dimuons. In next to leading order analyses the charm mass is closer to 1.5 GeV). For ξ_w the parameter A is expected to be much smaller than for x_w since now it only accounts for the higher order (dynamic higher twist) QCD terms in the form of an *enhanced* target mass term (the effects of the proton target mass are already taken into account using the exact form in the denominator of ξ_w). The parameter B accounts for the initial state quark transverse momentum and final state quark *effective* $\Delta {M_f}^2$ (originating from multi-gluon emission by quarks).

Using closure considerations [52] (*e.g.*the Gottfried sum rule) and the Adler sum rule, it can be shown that, at low Q^2, the scaling prediction for the *valence* quark part of F_2 should be multiplied by the factor K=[1-$G_D^2(Q^2)$][1+M(Q^2)] where $G_D = 1/(1+Q^2/0.71)^2$ is the proton elastic form factor, and M(Q^2) is related to the magnetic elastic form factors of the proton and neutron. At low Q^2, [1-$G_D^2(Q^2)$] is approximately $Q^2/(Q^2$ +C) with $C = M_V^2/4 = 0.71/4 = 0.178$ (versus the fit value of C=0.18 with GRV94). In order to satisfy the Adler Sum rule [4] the function M(Q^2) is added to account for terms from the magnetic elastic form factors of the nucleon). Therefore, a more general form $K_{valence-vector}$=[1-$G_D^2(Q^2)$][Q^2+C_{2v}]/[Q^2 +C_{1v}], and $K_{sea-vector}$=Q^2/(Q^2+C_{sea}) is used. Using this form with the GRV98 PDFs (and now also including the very low x NMC and H1 94 data in the fit) yields A=0.419, B=0.223, and C_{1v}=0.544, C_{2v}=0.431, and C_{sea}=0.380 (all in GeV^2, χ^2 = 1235/1200 DOF).

As expected, A and B are now smaller with respect to the previous fits with GRV94 and x_w. With these modifications, the GRV98 PDFs must also be multiplied by N=1.011 to *normalize* to the SLAC F_{2p} data. The fit (Figure 18) yields the following normalizations relative to the SLAC F_{2p} data ($SLAC_D$=0.986, $BCDMS_P$=0.964, $BCDMS_D$=0.984, NMC_P=1.00, NMC_D=0.993, $H1_P$=0.977, and BCDMS systematic error shift of 1.7).(Note, since the GRV98 PDFs do not include the charm sea, for $Q^2 > 0.8$ GeV^2 charm production is included using the photon-gluon fusion model in order to fit the very high ν HERA data. This is not needed for any of the low energy comparisons but is only needed to describe the highest ν HERA electro and photoproduction data).

Comparisons of *predictions* using these modi-

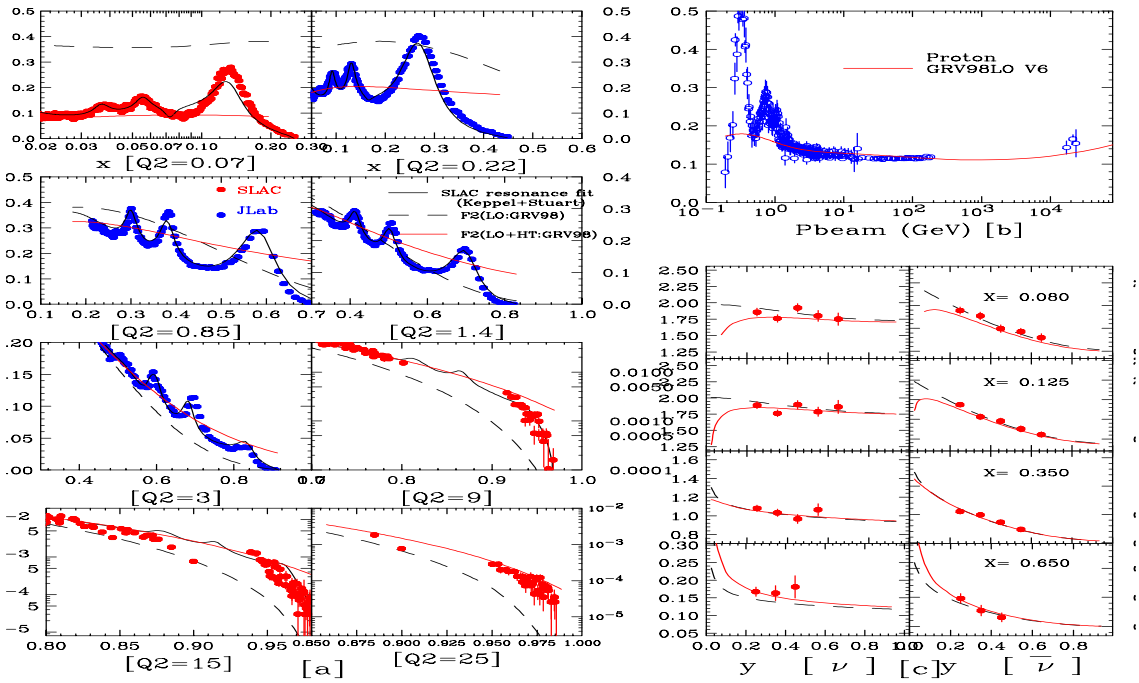

Figure 19. Comparisons to proton and iron data not included in the Bodek-Yang GRV98 ξ_w fit. (a) Comparison of SLAC and JLab (electron) F_{2p} data in the resonance region (or fits to these data) and the predictions of the GRV98 PDFs with (LO+HT, solid) and without (LO, dashed) our modifications. (b) Comparison of photoproduction data on protons to predictions using our modified GRV98 PDFs. (c) Comparison of representative CCFR ν_μ and $\overline{\nu}_\mu$ charged-current differential cross sections [44,53] on iron at 55 GeV and the predictions of the GRV98 PDFs with (LO+HT, solid) and without (LO, dashed) our modifications.

fied GRV98 PDFs to other data which were *not included* in the fit are shown in Figures 19 and 20. From duality [54] considerations, with the ξ_w scaling variable, the modified GRV98 PDFs should also provide a reasonable description of the average value of F_2 in the resonance region. Figures 19(a) and 20(a) show a comparison between resonance data (from SLAC and Jefferson Lab, or parametrizations of these data [55]) on protons and deuterons versus the predictions with the standard GRV98 PDFs (LO) and with the modified GRV98 PDFs (LO+HT). The modified GRVB98 PDFs are in good agreement with SLAC and JLab resonance data down to $Q^2 = 0.07$ (although resonance data were not included in the fits). There is also very good agreement of the *predictions* of the modified GRV98 in the $Q^2 = 0$ limit with photoproduction data on protons and deuterons as shown in Figure 19(b) and 20(b). In predicting the photoproduction cross sections on deuterium, shadowing corrections [59] were applied as shown in Figure 20(c). The *predictions* with the modified GRV98 PDFs (LO+HT) are also compared to a few representative high energy CCFR ν_μ and $\overline{\nu}_\mu$ charged-current neutrino differential cross sections [44,53] on iron (neutrino data were not included in the fit). In this comparison the PDFs are used to obtain F_2 and xF_3 and corrected for nuclear effects in iron [48]. The structure function $2xF_1$ is ob-

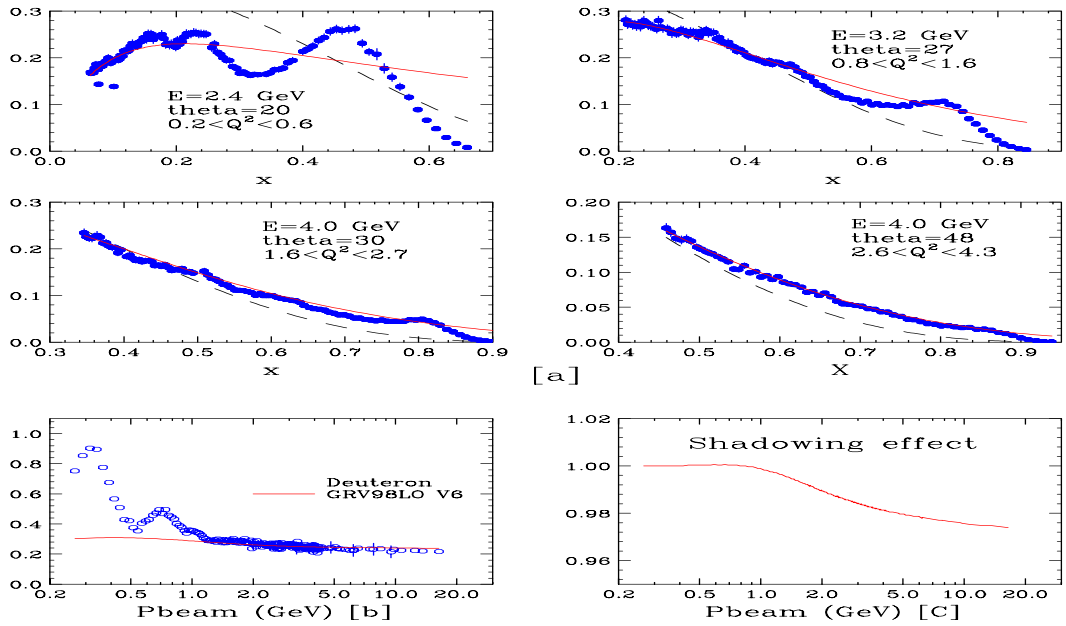

Figure 20. Comparisons to data on deuterium which were not included in the Bodek-Yang GRV98 ξ_w fit. (a) Comparison of SLAC and JLab (electron) F_{2d} data in the resonance region and the predictions of the GRV98 PDFs with (LO+HT, solid) and without (LO, dashed) our modifications. (b) Comparison of photoproduction data on deuterium to predictions using the Bodek-Yang modified GRV98 PDFs (including shadowing corrections). (c) The shadowing corrections that were applied to the PDFs for predicting the photoproduction cross section on deuterium.

tained by using the R_{world} fit from reference [45]. In addition, for this comparison we have assumed that $K_{valence-axial}$=$K_{valence-vector}$, and $K_{sea-axial}$=$K_{sea-vector}$. This assumption is expected to be valid at high Q^2, but is expected to break down as Q^2 approaches zero [51] (as discussed in a following section). There is very good agreement of the Bodek-Yang *predictions* with these high energy neutrino data on iron.

13. Using the Adler Sum Rules and Axial Structure Functions

One of the long term goals of modeling electron and neutrino scattering at all energies is to be able to test the Adler [4] sum rules. The Adler sum rules are Current-Algebra sum rules that are expected to be valid for all values of Q^2 from Q^2= 0 to the highest values Q^2

Other sum rules such as (a) the Energy-Momentum Sum-Rule (sum of quark and gluon fractional mometum = 1); (b) The Bjorken Sum-Rule, (c) The Gottfried Sum-Rule [52] and (d) the Gross-Llewyllyn-Smith Sum-Rule (number of valence quarks equal to 3), all have QCD corrections and break down at low values of Q^2. Therefore, a successful model of structure functions must satisfy the QCD sum rules at high Q^2, and the Adler sum-rules at *all values* of Q^2. In all of these sum rules, the elastic contribution needs to be included. As discussed earlier, Bodek and Yang use the Adler sum rule for the vector part of W_2 to obtain an expression for the low Q^2 K factor multiplicative factor to the GRV98 PDFs in the case of vector scattering. Here we show that a different K factor is expected for the case

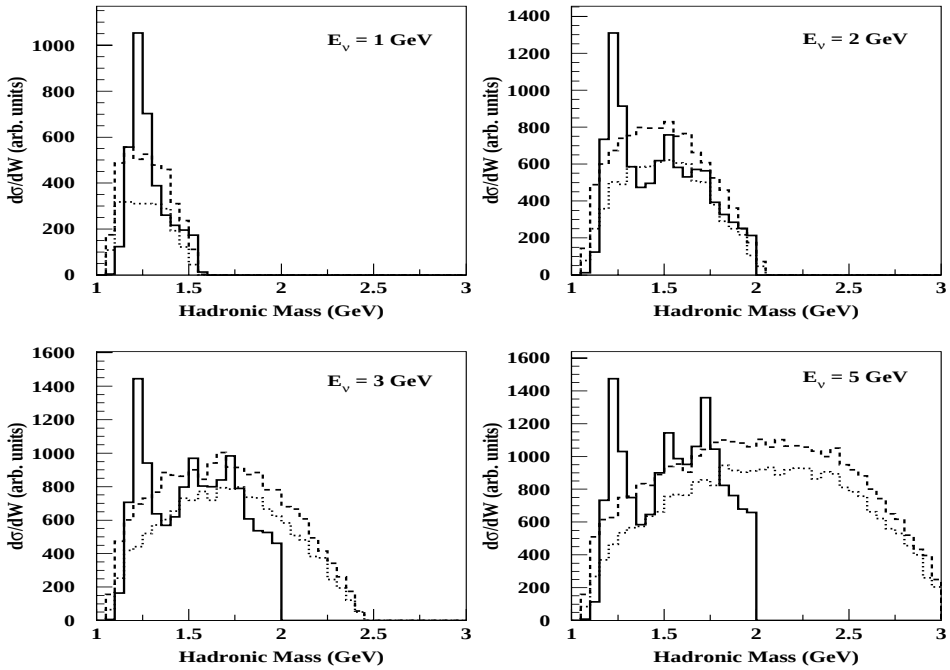

Figure 21. Comparison the prediction of the distribution in W (in the resonance region) for the R-S model to the predictions from the Bodek-Yang GRV98 modified PDFs (for neutrino energies of 2, 3 and 5 GeV). for different assumptions about the K factor for axial scattering. The solid line is the Rein-Sehgal prediction. The dotted line is the Bodek-Yang predictions assuming (incorrectly) $K_{valence-axial}$=$K_{valence-vector}$, and $K_{sea-axial}$=$K_{sea-vector}$. The dashed line is the Bodek-Yang prediction with the K factors for axial scattering with Z=0.5. (D. Casper-private communication)

of axial scattering.

We use the first two β Adler sum rules for the structure function W_2. Here β_p^-=W_{2p}^- and β_p^+=W_{2p}^+ refers to antineutrino-proton and neutrino-proton (strangeness conserving $\Delta S = 0$) structure functions respectively. At high Q^2 the basic quark model interpretation of these two Adler sum rules is that the number of valence u quarks minus the number of valence d quarks is 2-1=1 (for either vector or axial scattering). For all Q^2, these two sum rules are integrals from $\nu = q_0 = 0$ to $\nu = \infty$, and $q = [1/(cos^2\theta_c)]$:

$$\int_0^\infty q \left[W_{2p\Delta S=0}^{vec-}(\nu, q^2) - W_{2p\Delta S=0}^{vec+}(\nu, q^2) \right] d\nu = 1$$

$$\int_0^\infty q \left[W_{2p\Delta S=0}^{ax-}(\nu, q^2) - W_{2p\Delta S=0}^{ax+}(\nu, q^2) \right] d\nu = 1$$

If we separate out the quasielastic delta function contributions the above two equations become.

$$|F_V(q^2)|^2 + \int_{\nu_0}^\infty q \left[W_{2p\Delta S=0}^{vec-}(\nu, q^2) - W_{2p\Delta S=0}^{vec+}(\nu, Q^2) \right] d\nu = 1$$

$$|F_A(q^2)|^2 + \int_{\nu_0}^\infty q \left[W_{2p\Delta S=0}^{ax-}(\nu, q^2) - W_{2p\Delta S=0}^{ax+}(\nu, Q^2) \right] d\nu = 1$$

Where the limits of the integrals are from pion threshold ν_0 where $W = M_\pi + M_P$ to infinity. Here

$$|F_V(q^2)|^2 = |F_V^1(q^2)|^2 - \frac{q^2}{M^2}\left|\frac{\xi F_V^2(q^2)}{2}\right|^2$$

$$F_A(q^2) = \frac{g_A}{\left(1-\frac{q^2}{M_A^2}\right)^2}$$

$$F_V^1(q^2) = \frac{G_E^V(q^2) - \frac{q^2}{4M^2}G_M^V(q^2)}{1-\frac{q^2}{4M^2}},$$

$$\xi F_V^2(q^2) = \frac{G_M^V(q^2) - G_E^V(q^2)}{1-\frac{q^2}{4M^2}}.$$

$$q^2 = q_0^2 - \vec{q}_3^2 = -4E_0E'\sin^2\frac{\theta}{2} = -Q^2 \ .$$

At Q^2=0 we have $|F_V(q^2)|^2$=1 and $|F_A(q^2)|^2$=g_a^2=1.605. Therefore, in this limit the inelastic vector structure functions must go to zero, while the inelastic axial structure function remain finite. Note that the above sum rule only holds for the case of strageness conserving process which consist of 95% of the cross section in neutrino scattering. For the strangeness changing processes which consist of 5% of the cross section, the corresponding Adler sum rule (discussed at the end of this talk) indicates that the production of strange resonances is not suppresed at Q^2=0. This difference has not yet been implemented in the Bodek-Yang model.

For the vector structure functions, for which there is a multitude of data, we used the form $K_{valence-vector}$=[1-$G_D^2(Q^2)$][Q^2+C_{2v}]/[Q^2 +C_{1v}], and $K_{sea-vector}$=Q^2/(Q^2+C_{v-sea}). Using this form with the GRV98 PDFs (and now also including the very low x NMC and H1 94 data in the fit) yields A=0.419, B=0.223, and C_{1v}=0.544, C_{2v}=0.431, and C_{v-sea}=0.380 (all in GeV^2)

For the axial structure function, we first derive the general form that should satisfy the Adler axial sum rule. To satisfy the sum rule in the axial case, the K factors for the axial valence u and d quarks must be different (and could also be different for the axial sea).

$$K_{ax-Uv} = [Q^2 + C_{2ax-Uv}]/[Q^2 + C_{1ax-v}],$$

$$K_{ax-Dv} = [Q^2 + C_{2ax-Dv}]/[Q^2 + C_{1ax-v}],$$

The above K factors for the U and D valence quarks become 1.0 at high Q^2. Therefore, this form automatically satisfies Adler sum rules at infinite Q^2. Note, however, that this form assumes that all the K factors are independent of W (which is only an approximation). Plugging the above forms into the Adler Axial sum rule and expanding for very low Q^2 yields a constant term and a term linear in Q^2. Requiring the axial sum rule to be valid at Q^2=0 and also at very small Q^2 yields (to within an overall scale factor Z, which should be less than 1):

$$C_{1ax-v} = M_A^2/4 = 0.25\ GeV^2$$

$$C_{2ax-Uv} = ZC_{1ax-v} = Z(0.25)\ GeV^2$$

$$C_{2ax-Dv} = [2Z + (g_a^2 - 1)[C_{1ax-v}]$$

$$= [2Z + 0.605)0.25\ GeV^2$$

For Z = 0.1 we get C_{2ax-Uv}=0.025 GeV^2 and C_{2ax-Dv}= 0.113 GeV^2. For Z = 0.5 we get C_{2ax-Uv}=0.125 GeV^2 and C_{2ax-Dv}= 0.40 GeV^2. (within this model, the value of Z needs to be extracted from fits to CHORUS, CCFR, CDHS and other low energy neutrino data)

Note that the K factor for the axial sea is not constrained by the Adler sum rule and the sea parameters need to be extracted from fits to neutrino data. K_{ax-sea} = [Q^2 + D_{ax-sea}]/[Q^2 + C_{ax-sea}]. for now, we just use the average of the valence parameters used for the axial valence quarks. i.e. for Z=0.1, C_{ac-sea}=0.25 GeV^2 and D_{ax-sea}=0.113 GeV^2 . For Z=0.5, C_{ac-sea}=0.25 GeV^2 and D_{ax-sea}=0.263 GeV^2. The axial K factors are rather insensitive to the value of M_A, and mostly depend on the vallue of Z. An expanded discussion of sum rules is presented in a later section (section 21).

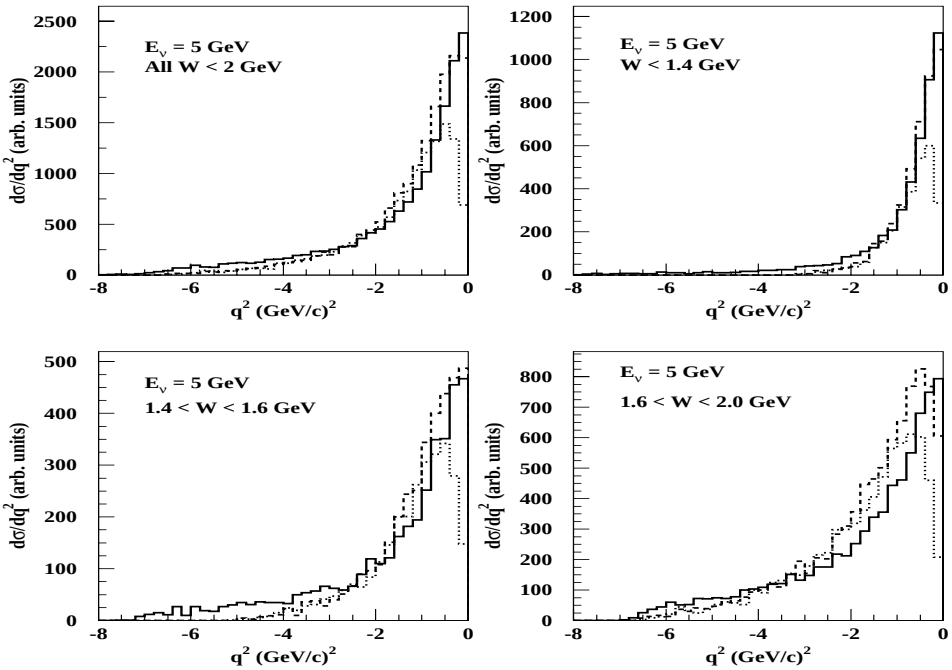

Figure 22. The Q^2 distributions (for a fixed neutrino energy of 5 GeV) are shown for different bins in W. The solid line is the Rein-Sehgal prediction. The dotted line is the Bodek-Yang prediction assuming (incorrectly) $K_{valence-axial}$=$K_{valence-vector}$, and $K_{sea-axial}$=$K_{sea-vector}$. The dashed line is the Bodek-Yang prediction with the K factors for axial scattering with Z=0.5. (D. Casper-private communication)

14. Comparison of Bodek-Yang PDFs to the Rein-Sehgal Resonance Model

Resonance production is discussed in detail in a later section. As was shown in the the previous section, the Bodek-Yang model provides a good description of the average vector cross sections in the resonance region for the case of electron scattering. However, since low energy neutrino data have not yet been included in the Bodek-Yang fits, the axial structure functions are not yet finalized. Therefore, it is of interest to compare the Bodek-Yang predictions in the resonance region that of the Rein-Seghal model. The Rein-Seghal model is an old fit to low energy data for the electroproduction and neutrino production of resonances within a quark oscillator model. The model includes an an axial form factor for resonance which is similar to the axial form factor in quasielastic scattering.

Figure 21 (from D. Casper) compares the prediction of the distribution in W (in the resonance region) for the Rein-Sehgal model to the predictions from the Bodek-Yang GRV98 modified PDFs (for neutrino energies of 2, 3 and 5 GeV). The comparison is done for two different assumptions about the K factor for axial scattering. The solid line is the Rein-Sehgal prediction. The dotted line is the Bodek-Yang prediction assuming (incorrectly) $K_{valence-axial}$=$K_{valence-vector}$, and $K_{sea-axial}$=$K_{sea-vector}$. The dashed line is the

Bodek-Yang prediction with the K factors for axial scattering (described above) with Z=0.5. As can be seen from the figure, there is reasonable agreement in the region of the second and third resonances (as expected from duality) between the two models if we include an axial contribution. Note that above W of 1.7 GeV , the Rein-Seghal model underestimates the cross section because the model does not include any resonances above $W = 2\ GeV$.

Figure 22 compares the Q^2 distributions (for a fixed neutrino energy of 5 GeV) in different bins in W. The solid line is the Rein-Sehgal prediction. The dotted line is the Bodek-Yang prediction assuming (incorrectly) $K_{valence-axial}$=$K_{valence-vector}$, and $K_{sea-axial}$=$K_{sea-vector}$. The dashed line is the Bodek-Yang prediction with the K factors for axial scattering (described above) with Z=0.5. A reasonable prescription is to use current implementation of Rein-Seghal model in the resonance region and use the Bodek-Yang modek (with an axial contribution) in above the resonance region. Note that the Bodek-Yang model needs to be coupled with the Lund fragmentation model to provide the composition of the hadronic final states). Additional remarks on resonance production are presented in section 18. A prescription for providing a cross section which is continuous in W is described in a later section (section 19).

15. The Longitudinal Structure Function R

In leading order QCD (e.g. GRV98 LO PDFs), F_2 for the scattering of electrons and muons on proton (or neutron) targets is given by the sum of quark and anti-quark distributions (each weighted the square of the quark charges):

$$F_2(x) = \Sigma_i e_i^2 \left[x q_i(x) + x\overline{q}_i(x)\right] \quad (1)$$

$$2xF_1(x) = F_2(x)(1+4Mx^2/Q^2)/(1+R_w) \quad (2)$$

In reality, a reconstruction of $2xF_1$ from the values of R and F_2 in neutrino scattering is not as simple as in the case of charged lepton scattering (because of charm production). For charm production, the Bjorken scaling variable x no longer represents the fractional momentum carried by the struck quark in the infinite momentum frame due to the non-zero heavy mass of the charm quark ($m_c \sim 1.3$ GeV). For charm production processes, the variable x is replaced by the slow rescaling variable $\xi = (1 + m_c^2/Q^2)x$. Therefore, the structure functions for the charm production (cp) and non-charm production (ncp) components are given by the following expressions.

$$F_2^{cp+ncp}(x) = F_2^{ncp}(x) + F_2^{cp}(\xi) \quad (3)$$

$$2xF_1^{cp+ncp}(x) = \frac{1+4M^2x^2/Q^2}{1+R^{ncp}(x)}F_2^{ncp}(x) + \frac{1+4M^2\xi^2/Q^2}{1+R^{ncp}(\xi)}F_2^{ncp}(\xi) \quad (4)$$

In this model, the R_w fit is used for R^{ncp} and R^{cp}, where $R_w(x,Q^2)$ is parameterized [45] by:

$$R_w = \frac{0.0635}{log(Q^2/0.04)}\theta(x,Q^2) + \frac{0.5747}{Q^2} - \frac{0.3534}{Q^4+0.09}, \quad (5)$$

where $\theta = 1. + \frac{12Q^2}{Q^2+1.0} \times \frac{0.125^2}{0.125^2+x^2}$.

The R_w function provides a good description of the world's data in the $Q^2 > 0.5$ and $x > 0.05$ region (see Figure 23) Note that the R_w function breaks down below $Q^2 = 0.3$. Therefore, the function is frozen at $Q^2 = 0.35$ and another function for R in the $Q^2 < 0.35$ region is used. The new function provides a smooth transition from $Q^2 = 0.35$ down to $Q^2 = 0$ by forcing R to approach zero at $Q^2 = 0$ as expected in the photoproduction limit (while keeping a $1/Q^2$ behavior at large Q^2 and matching to R_w at $Q^2 = 0.35$).

$$R = 3.207 \times \frac{Q^2}{Q^4+1} \times R_w(x, Q^2 = 0.35). \quad (6)$$

In neutrino scattering the value of R is required to approach zero at $Q^2 = 0$ only for the vector part of the interaction. Studies of the axial contribution at low Q^2 are currently under way.

A large unknown is the value of R in the resonance region for both vector and axial scattering, and also the nuclear effects on R in the resonance region at low Q^2. Figures 24, 25 26 show preliminary results of analysis of data from Jlab experiment E94-110 [38] on hydrogen. Data with

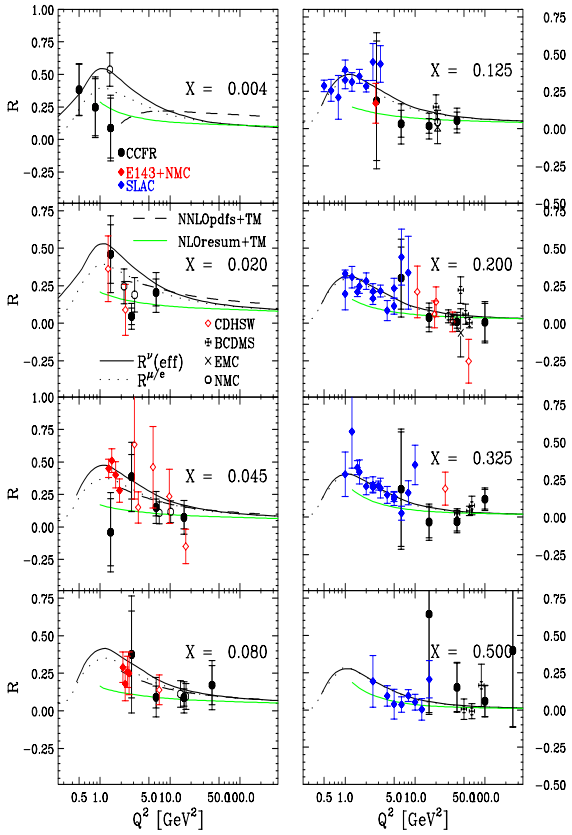

Figure 23. A compilation of the world's data on R [44,53].

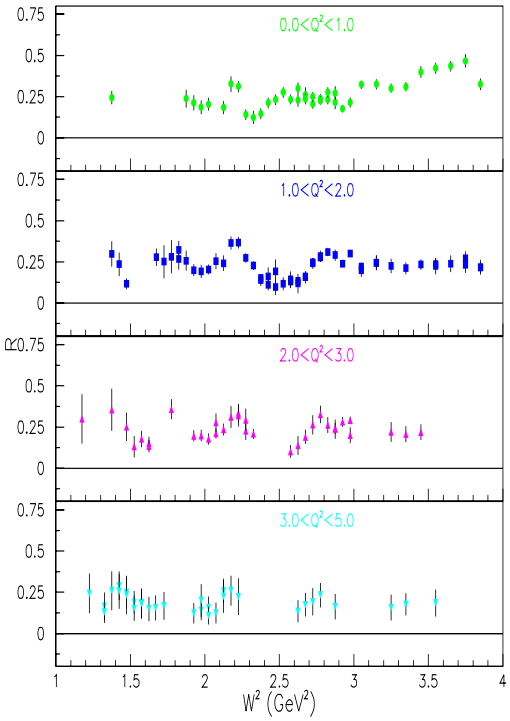

Figure 24. Recent data from Jlab experiment E94-110 (on hydrogen) for R in the resonance region. Data with deutrerium is expected to be taken in experiment E02-109, and data with nuclear target is proposed to be taken by P03-110.

deutrerium is expected to be taken in experiment E02-109, and data with nuclear target is proposed to be taken by P03-110. The resonance region is discussed in more detail at the end of this paper.

16. Inelastic Scattering, Corrections for Nuclear Binding Effects

In the comparison with CCFR charged-current differential cross section on iron, a nuclear correction for iron targets is applied. The following parameterized function, $f(x)$ (but substituting ξ_w for x) is used. This fit to the experimental electron and muon scattering data for the ratio of iron to deuterium cross sections in the DIS region (shown in Figure 27) is used to convert deuterium structure functions to (isoscalar) iron structure functions [48];

$$f(x) = 1.096 - 0.364x - 0.278e^{-21.94x} + 2.772x^{14.417} \quad (7)$$

Recent results from Jlab presented at this conference indicate that the Fe/D ratio in the resonance region is the same as the Fe/D ratio from DIS data for the same value of Nachtman target mass variable ξ (which is the same as ξ_w with A=0 and B=0). A comparison of the iron to deu-

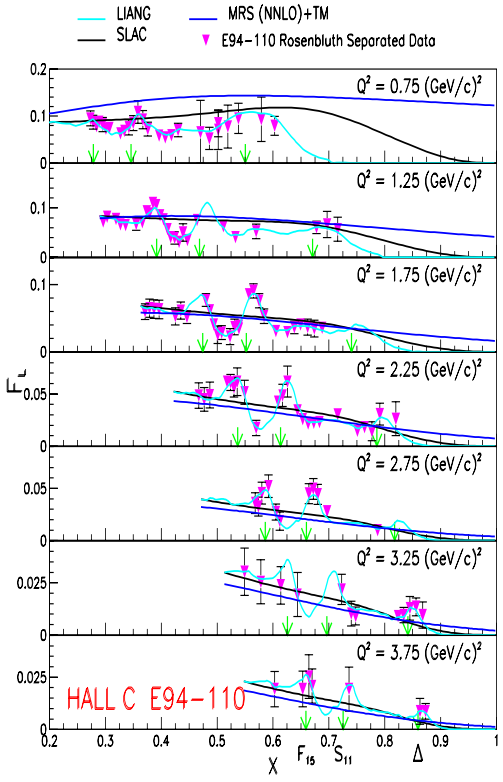

Figure 25. Recent data from Jlab experiment E94-110 (on hydrogen) for F_L in the resonance region. Data with deutrerium is expected to be taken in experiment E02-109, and data with nuclear target is proposed to be taken by P03-110.

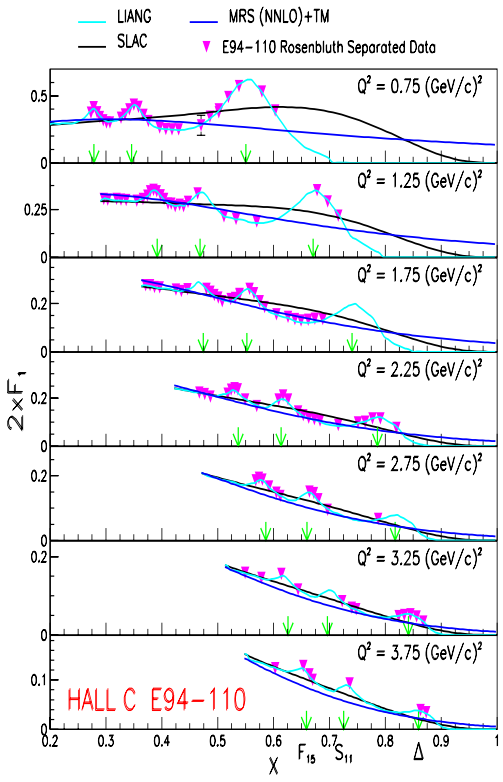

Figure 26. Recent data from Jlab experiment E94-110 (on Hydrogen) for $2xF_1$ in the resonance region. Data with deutrerium is expected to be taken in experiment E02-109, and data with nuclear target is proposed to be taken by P03-110.

terium ratio $f(x)$ in the deep-inelastic and in the resonance region (at higher Q^2), shown in Figure 28 indicates that in the resonance region, the ratio is the same in the resonance and DIS region if plotted in terms of the ξ . Note that the variable ξ is equal to ξ_w for large Q^2.

For the ratio of deuterium cross sections to cross sections on free nucleons we use the following function obtained from a fit to SLAC data on the nuclear dependence of electron scattering cross sections [44] (but substituting ξ_w for x).

$$f = (0.985 \pm 0.0013) \times (1 + 0.422x - 2.745x^2 + 7.570x^3 - 10.335x^4 + 5.422x^5). \quad (8)$$

This correction is only valid in the $0.05 < x < 0.75$ region. In neutrino scattering, we use the same nuclear correction factor for F_2, xF_3 and $2xF_1$.

Although all the above expression for R and the nuclear correction factor were parametrized in terms of the variable x, it is probably more correct to substitute the scaling variable ξ_w for

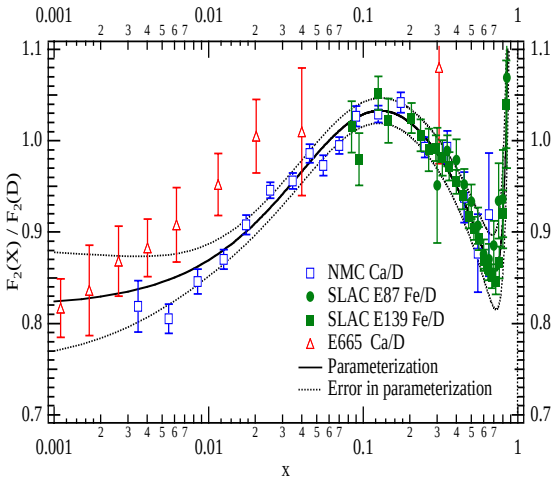

Figure 27. Deep-inelastic charged lepton data on the iron to deuterium ratio compared to the fit f(x) described in the text.

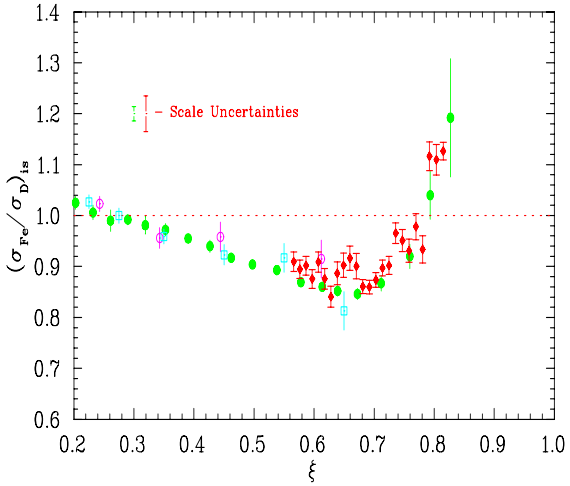

Figure 28. Comparison of the iron to deuterium ratio in the inelastic region and in the resonance region versus the target mass variable ξ

x in these expressions. Such a substitution will make the expression more valid at low W and low Q^2.

17. Other Corrections to GRV98 PDFs

The d/u correction for the GRV98 LO PDFs is obtained from the NMC data for F_2^D/F_2^P. Here, Eq. 8 is used to remove nuclear binding effects in the NMC deuterium F_2 data. The correction term, $\delta(d/u)(x)$ is obtained by keeping the total valence and sea quarks the same.

$$\delta(d/u) \quad = \quad -0.00817 + 0.0506x + 0.0798x^2, \quad (9)$$

where the corrected d/u ratio is $(d/u)' = (d/u) + \delta(d/u)$. Thus, the modified u and d valence distributions are given by

$$u'_v = \frac{u_v}{1 + \delta(d/u)\frac{u_v}{u_v+d_v}} \quad (10)$$

$$d'_v = \frac{d_v + u_v\delta(d/u)}{1 + \delta(d/u)\frac{u_v}{u_v+d_v}}. \quad (11)$$

The same formalism is applied to the modified u and d sea distributions. Accidently, the modified u and d sea distributions (based on NMC data) agree with the NUSEA data in the range of x between 0.1 and 0.4. Thus, we find that any further correction on sea quarks is not necessary.

18. Resonance Production

As mentioned earlier the value of R in the resonance region for both vector and axial scattering is not known very well. In addition, the axial part of F_2 and xF_3 are not well known. Also, the nuclear effects of R in the resonance region at low Q^2 and W has not been measured in either vector or axial scattering.

Figures 24, 25 and 26 show preliminary results of analysis of data on R from Jlab experiment E94-110 [38] on hydrogen. These high precision measurements will be extended to deuterium by Jlab experiment E02-109 [39] (to run sometimes in 2004). In addition, there is a proposal to add measurements from nuclear targets at the same time (see Jlab proposal E03-110 [41]). Therefore, after these experiments are run, it is expected that data from the following Jlab experiments experiments in the resonance region: E94-110 (H), E02-109 (D), E02-103 (H and D at high Q^2) and

nuclear target experiment P03-110 [41] will provide detailed information on the vector structure functions (both F_2 and R) for H, D and nuclear targets in the resonance region. In addition, Jlab nuclear target experiment E99-118 [40] measured the low Q^2 values of $F2$ and R above the resonance region. Precision measurments of the corresponding axial structure functions in this low energy region will be done by MINERvA at Fermilab.

In neutrino scattering, the model of Rein and Sehgal [56] (R-S) is the model which is often used to simulate neutrino production of resonances. The R-S model is an old model built on the quark harmonic oscillator model of Feynman and Randal [56]. It has incorporated early data on the photoproduction and electroproduction of resonances in combination with the limited available data on resonance production in neutrino and antineutrino beams. The vector form factors were taken from electroproduction and related to neutrino production by Celbsch-Gordon rules.

The following are some of the advantages of the R-S model.

1. It relates the vector form factors of various resonances from fits of photoproduction and electroproduction data to both charged-current and neutral-current neutrino processes via Clebsch-Gordon coefficients for the various isopsin states of the resonances.

2. It models the axial form factors using neutrino data

3. It provides a description of the decay products of the hadronic final states.

4. It provides a framework for a simultaneous description of all leptoproduction processes (including whatever neutrino data exists) by modeling a very large number of resonances.

5. It has been implemented in a Monte Carlo simulation form.

6. It uses information from pion-nucleon scattering to constrain the various resonances (which is are not separable by using photoproduction and electropduction data only,

The following are some of the limitations of the R-S model.

1. The vector and axial resonance form factors are assumed to be similar to that of the quasielastic peak. Therefore it does not include the modifications due to the pion cloud.

2. Only the quark contribution to the longitudinal structure function and R are calculated. Therefore R is underestimated since it does not include the modifications due to the pion cloud. For example, the longitudinal structure functions R and F_L are predicted to be zero in the region of the first resonance. This result is is in disagreement with recent data from Jlab experiment E94-110, and requires that the effect of the pion cloud be included.

3. It does not include any resonances above a mass W of 2 GeV. Therefore, it breaks down at high energies and in the transition region between resonance and deep-inelastic scattering.

4. The inelastic continuum under the resonances is not very well modeled.

5. It is an old model which does not include any of the more recent electroproduction data and neutrino production in the fits.

6. It does not include nuclear corrections such as Fermi motion and final state interactions of the outgoing hadrons (but these may be added separately).

7. It does not include nuclear binding corrections to the resonance and continuum form factors (but these may be added separately).

8. The neutrino data that was used as input to constrain some of the parameters of the model is of rather poor quality.

As mentioned earlier the production in the region of the first resonance, the R-S model predicts $R = 0$ and $F_L = 0$ for vector/electrorpoduction. This is in disagreement with recent precision measurement from Jlab as shown in Figures 24 and 25. However, this flaw may be corrected, as done in the Bodek-Yang model, by adding an empirical contributinon to F_L as measured in electroproduction experiments.

Figure 29 shows the prediction from Sato and Lee [57] for the vector and axial form factors in neutrino production of the first Delta resonance. The solid line is the full calculation including the nucleon pion cloud. The dashed line is without the effects of the pion cloud (which is similar to what one expects in the R-S quark model).

Note that duality is expected to break down in neutrino and antineutrino reactions, in the region of the first and the quasielastic peak. This is because the $W = M$ and W=1.23 GeV regions are dominated by one and two isospin states, and the amplitudes for neutrino versus electron scattering are related via Clebsch-Gordon rules [56] instead of quark charges. For example, unlike the case for neutrino scattering from neutron target, is no quasielatic neutrino scattering from a proton target since the final state is a charge +2 resonance. Although local duality may work work better for the sum of neutrino and antineutrino scattering.

In addition, as already mentioned the V and A couplings are not equal at low W and Q^2. All these issues can be corrected when neutrino data is included in the Bodek-Yang fits for the axial structure functions.

In the region of higher mass resonances (e.g. W=1.8 GeV) there is a significant contribution from the deep-inelastic continuum which is not well modeled by the Rein-Seghal fits [56] to neutrino resonance data (which can be corrected if resonances with W $>$ 2 GeV are added to R-S in the future. Therefore, using the Bodek-Yang PDFs for $W > 1.8\ GeV$ (with an axial contribution) should be better. For nuclear targets, the nuclear corrections [48] described earlier must also be applied.

19. Combining Quasielastic Resonance and Inelastic Contributions

In order to have a full description of all charged current ν_μ and $\overline{\nu}_\mu$ processes, the contribution from quasielastic scattering [2] must be added separately at $x = 1$.

For W above the quasielastic peak, the three available models (Bodek-Yang, Rein- Sehgal and Sato-Lee) all have problems in different W regions (and all need to be improved). At present it is best to use the Sato-Lee [57] model for the first resonance, the Rein-Sehgal model in the region of the second and third resonances and the Bodek-Yang model (coupled with a Lund fragmentation for final states) in the region above the third resonance. Note that because of the effects of experimental resolution and Fermi motion [34] (for nuclear targets), a description of the average cross section in the region of higher resonances is sufficient for most neutrino experiments. Figure 30 shows the total neutrino cross section (per nucleon for an isoscalar target) versus energy (at low energies) compared to the sum of quasielastic, resonance, and inelastic contributions from D. Casper. The sum is constructed to be continuous in W as follows. For $W > 2\ GeV$ the Bodek-Yang model is used with the axial structure functions calculated with $Z = 0.5$. The Rein-Sehgal model is used used for $W < 2\ GeV$. In addition, a fraction of the Bodek-Yang cross section is added to the Rein-Sehgal cross section between $W = 1.7\ GeV$ and $W = 2\ GeV$. The fraction increases linearly with W from 0 to 0.38 between W=1.7 and 2 W=2 GeV. This prescription gives pretty good agreement with the measured total cross-section, and provides a continuous W distribution between the resonance and inelastic regions.

The effects of terms proportional to the muon mass and F_4 and F_5 structure functions in neutrino scattering are small and are discussed in Ref. [2,58].

For completenes, Figures 31 and 32 show the total neutrino and antineutrino cross sections (per nucleon for an isoscalar target devided by neutrino energy) versus energy in the high energy region.

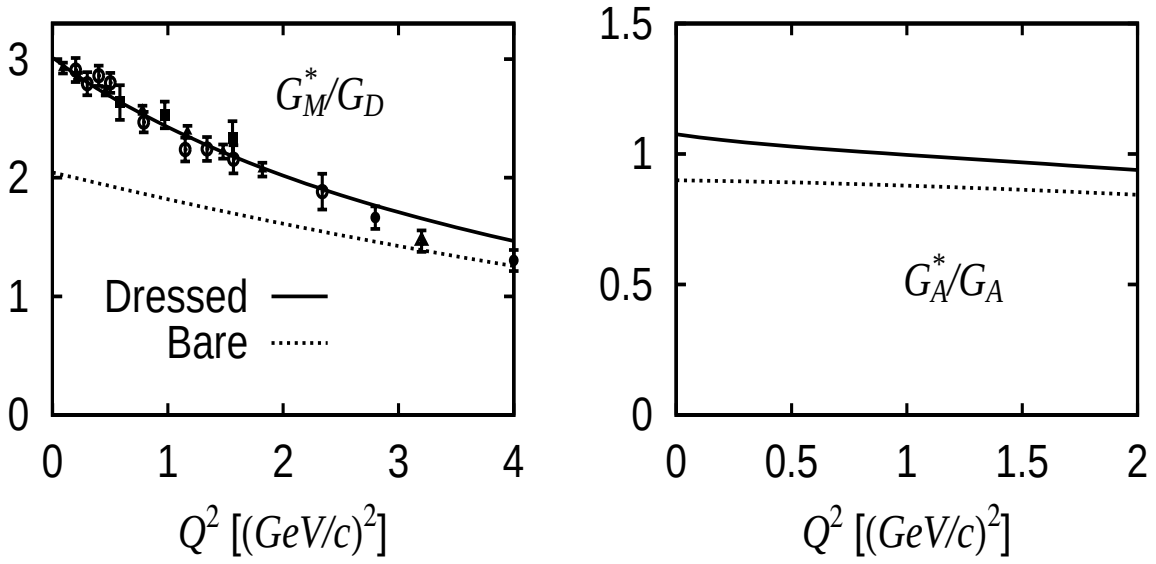

Figure 29. Magnetic and axial form factors for neutrino production in the Delta resonance region from the calculation of Sato and Lee [57] . The solid line is the full calculation including the nucleon pion cloud. The dashed line is without the effects of the pion cloud.

20. Outlook for the future

A worthwhile aim is to improve the Sato-Lee, Rein-Sehgal and Bodek-Yang models (and hopefully more in the future) to agree with each other (and with all existing data) over a large region of overlap in W. If this is accomplished, the predicted cross sections will be continuous in the transition region between the deep inelastic and resonance regions.

A. Improvements to the Sato-Lee Model.

There are current plans to extend the model of Sato and Lee (which is only available in the region of the first resonance) to the higher resonances. Since the model includes both quarks states and meson clouds, it should work better than the R-S model. However, the R-S model includes a very large number of resonances, and large volume of exclusive electroroduction data is needed to constrain these resonance parameters within the Sato and Lee model. Therefore it may be easier to improve on the R-S model by using information learned from the Sato and Lee fits for the first resonance.

B. Improvements to the Rein and Sehgal model.

1. Improve the resonance parameters by repeating the fits using more up to date data from Jlab in the resonance region.

2. Apply corrections for the missing terms from the pion cloud (guided by the Sato-Lee model) to improve the modeling of the vector and axial form factors.

3. Use new electroproduction data on R and F_2 from Jlab to improve the modeling of the continuum.

4. Improve he modeling of R

5. Include resonances and continuum with W $>$ 2 GeV (so the model works for higher values of W).

6. One could use the Sato-Lee model for the first resonance and the Rein-Seghal model

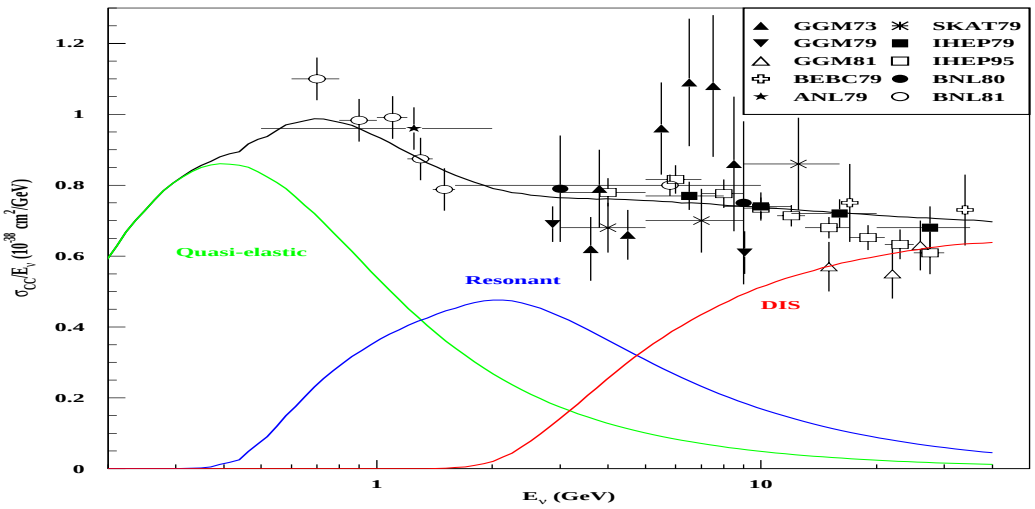

Figure 30. Total neutrino and antineutrino cross sections versus energy compared to the sum of quasielastic, resonance, and inelastic contributions, see text (from D. Casper, Private Communication)

for the remaining resonances.

C. Improvements to the Bodek-Yang Model

1. At very low Q^2, the vector structure function for changing conserving processes must go to zero, while the axial-vector part is finite. Plans are to including low energy data from Chorus (on Pb), CDHS and CCFR (in Fe) and other neutrino data in the fit, in order to constrain the low Q^2 axial-vector contribution, as previously discussed.

2. For strangeness-changing processes which consist of 5% of the cross section, the corresponding Adler sum rule (discussed at the end of this talk) indicates that the production of strange resonances is not suppresed at Q^2=0. This difference needs to be implemented in the Bodek-Yang model.

3. Improve the fit for the longitudinal structure function R for vector scattering, by including new data taken on Hydrogen from Jlab experiment E94-110.

4. Improve the description of the axial contribution to the longitudinal structure function.

5. The PDFs can be multiplied by a modulating function [50,52] A(W,Q^2) to improve modeling in the resonance region (for hydrogen) by including (instead of *predicting*) the resonance data [55] in the fit. One can also include resonance data on deuterium [55] and heavier nuclear targets in the fit, and low energy neutrino data.

6. In the future, there are plans to investigate the effects of including the initial state quark P_T in ξ_w, and institute further improvements such as allowing for different higher twist parameters for u, d, s, c, b quarks in the sea.

D. New electron scattering experiments that can be used to improve the models.

1. JLab hydrogen experiment E94-110 (investigate F_2 and R in the resonance region).

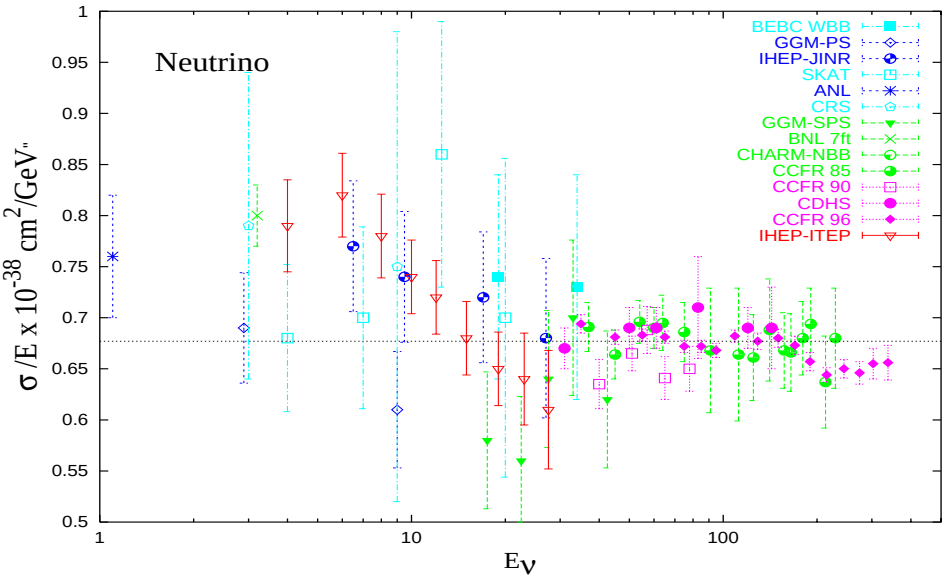

Figure 31. Total neutrino cross sections (per nucleon for an isoscalar target devided by neutrino energy) versus energy in the high energy region (from PDG, see talk by Donna Naples, this conference)

C.E. Keppel spokesperson (data already taken).

2. JLab deuterium experiment E02-109, investigate F_2 and R in the resonance region). C.E. Keppel, M. E. Christy, spokespersons (approved to run in 2004).

3. JLab experiment E99-118 on the nuclear dependence of R at low Q^2 for high values of W. A. Brull, C.E. Keppel spokespersons (data already taken).

4. Jlab experiment E02-103 hydrogen and deuterium resonance F_2 data at high Q^2 (and EMC effect in He3, He4) - approved by Jlab PAC24 to run in 2004 (J. Arrington, spokesperon)

5. Jlab Proposal PR03-110 to investigate F_2 and R in the resonance region with nuclear targets. A. Bodek and C. E. Keppel, spokespersons (proposed to run in Hall C together with E02-109 in 2004) to provide vector resonance form factors and R on nuclear targets for use in neutrino experiments (collaborate with MINERvA).

6. Steve Manly (Rochester) and Will Brooks (Jlab) proposal to CLAS collaboration to study hadronic final states in electron scattering on nuclear targets using existing Jlab Hall B CLAS data. This analysis will provide information on hadronic final states in quasielastic and inelastic electron scattering (for use in neutrino experiments and collaborate with MINEvA)

E. Current and future neutrino near detector experiments

1. K2K: Near detector; fully active scintillator (carbon) neutrino detector currently taking data in 2003 with 1-2 GeV neutrinos at KEK (low flux).

2. MiniBoone: (carbon) neutrino detector currently taking data in 2003 with 0.7 GeV neutrinos in the Fermilab Booster Beam.

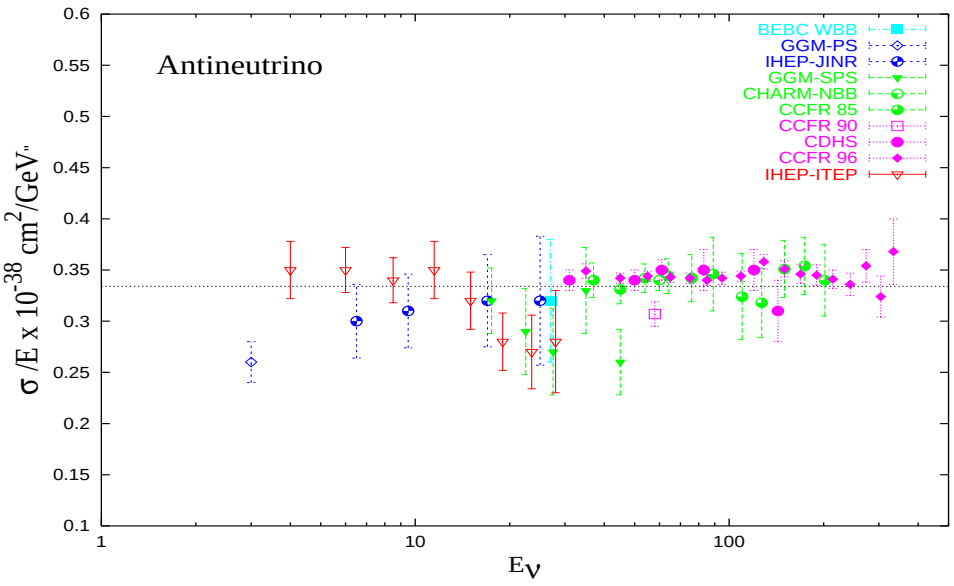

Figure 32. Total neutrino cross sections the total neutrino and antineutrino cross sections (per nucleon for an isoscalar target devided by neutrino energy) versus energy in the high energy region (from PDG, see talk by Donna Naples, this conference)

3. MINOS: iron-scintillator neutrino near detector. Currently being constructred to run in the high flux NUMI neutrino beam at Fermilab (between 2-8 GeV).

4. MINERvA: A fully active scintillator (carbon) near detector proposed to run in both on-axis and off-axis configuration in the NUMI neutrino beam at Fermilab (between 2-8 GeV). K. McFarland (Rochester), J. Morfin (Fermilab) and C. Keppel (Hampton/Jlab) spokespersons (collaborate with Jlab experiments listed above).

5. JPARC: Near detector; fully active scintillator (carbon) neutrino detector to take data with 1-2 GeV neutrinos to run at the new JHF facility in Japan.

21. Testing Sum Rules

One of the long term goals of modeling electron and neutrino scattering at all energies is to be able to test various sum rules over a large range of Q^2. For example, testing the Adler and Gilman [4] sum rules. The Adler sum rules are Current-Algebra sum rules that are expected to be valid for all values of Q^2 from Q^2= 0 to Q^2=∞.

We have used one of the Adler sum rules to guide us on the choice of functional forms for our fits for the vector and axial K factors. When a large amount of electron and neutrino scattering data are available, the models can be tested to see if they satisfy the various Adler sum rules. These sum rules are integrals from $\nu = q_0 = 0$ to $\nu = \infty$ (including the elastic/quasielastic contribution). The functions α, β and γ as defined by Adler correspond to the structure functions W_1 ,W_2, and W_3 in modern notation. Here W_1^-=α^-, W_2^-= β^- and W_3^-=γ^- refer to antineutrino structure functions, and W_1^+=α^+, W_2^+=β^+ and W_3^+=γ^+ refer to neutrino structure functions, respectively. If no subscripts are used then we refere to scattering on protons. Otherwise the subscripts p and n refer to scattering from protons and neutrons respectively. The superscripts vec and ax refer

to vector and axial scattering respectively. There are many Adler sum rules for the three structure functions on neutrons and protons and for the cases of strangeness-conserving and strangeness-changing processes. At high Q^2 all of the β sum rules are equivalent to the statement that the number of valence u quarks is =2 and the number of valence d quarks is =1. A few examples are shown below.

The following are the Adler sum rules for strangeness conserving charged-current reactions for $\beta_{p\Delta S=0}$:

$$\int_0^\infty \left[\beta^{vec-}_{p\Delta S=0}(\nu,q^2) - \beta^{vec+}_{p\Delta S=0}(\nu,q^2)\right] d\nu = cos^2\theta_c$$

$$\int_0^\infty \left[\beta^{ax-}_{p\Delta S=0}(\nu,q^2) - \beta^{ax+}_{p\Delta S=0}(\nu,q^2)\right] d\nu = cos^2\theta_c$$

The following are the Adler sum rules for strangeness conserving charged-current reactions for $\beta_{n\Delta S=0}$:

$$\int_0^\infty \left[\beta^{vec-}_{n\Delta S=0}(\nu,q^2) - \beta^{vec+}_{n\Delta S=0}(\nu,q^2)\right] d\nu = -cos^2\theta_c$$

$$\int_0^\infty \left[\beta^{ax-}_{n\Delta S=0}(\nu,q^2) - \beta^{ax+}_{n\Delta S=0}(\nu,q^2)\right] d\nu = -cos^2\theta_c$$

The following are the Adler sum rules for strangeness changing charged-current reactions for $\beta_{p\Delta S\pm1}$:

$$\int_0^\infty \left[\beta^{vec-}_{p\Delta S\pm1}(\nu,q^2) - \beta^{vec+}_{p\Delta S\pm1}(\nu,q^2)\right] d\nu = 2sin^2\theta_c$$

$$\int_0^\infty \left[\beta^{ax-}_{p\Delta S\pm1}(\nu,q^2) - \beta^{ax+}_{p\Delta S\pm1}(\nu,q^2)\right] d\nu = 2sin^2\theta_c$$

The following are the Adler sum rules for strangeness changing charged-current reactions for $\beta_{n\Delta S\pm1}$:

$$\int_0^\infty \left[\beta^{vec-}_{n\Delta S\pm1}(\nu,q^2) - \beta^{vec+}_{n\Delta S\pm1}(\nu,q^2)\right] d\nu = sin^2\theta_c \ .$$

$$\int_0^\infty \left[\beta^{ax-}_{n\Delta S\pm1}(\nu,q^2) - \beta^{ax+}_{n\Delta S\pm1}(\nu,q^2)\right] d\nu = sin^2\theta_c \ .$$

At high Q^2 the above four vector/axial pairs of equations are equivalent to a difference between pairs of equations below. i.e. equations 1 - 2 ($u_v - d_v = 1$), , equations 2 - 3 ($d_v - u_v = -1$), equations 5 - 6 (u_v=2) , and equations 7 - 8 ($d_v = 1$). (Here + denotes neutrinos and − denotes antineutrinos)

1. $\beta^-_{p\Delta S=0} = cos^2\theta_c[u+\overline{d}]+(Neutron = udd)$
2. $\beta^+_{p\Delta S=0} = cos^2\theta_c[d+\overline{u}]$
3. $\beta^-_{n\Delta S=0} = cos^2\theta_c[d+\overline{u}]$
4. $\beta^+_{n\Delta S=0} = cos^2\theta_c[u+\overline{d}]\ +(Proton = uud)$
5. $\beta^-_{p\Delta S\pm1} = [sin^2\theta_c u + cos^2\theta_c\overline{s}]+(\Lambda^0\ and\ \Sigma^0 = usd)$
6. $\beta^+_{p\Delta S\pm1} = cos^2\theta_c s + sin^2\theta_c\overline{u}$
7. $\beta^-_{n\Delta S\pm1} = [sin^2\theta_c d + cos^2\theta_c\overline{s}]+(\Sigma^- = dds)$
8. $\beta^+_{n\Delta S\pm1} = cos^2\theta_c s + sin^2\theta_c\overline{d}$

At Q^2=0 some of the above equations have discrete contributions at $W = M$ (for strangeness conserving $\beta^-_{p\Delta S=0}$ and $\beta^+_{n\Delta S=0}$) and at $W = M_\Lambda$ and $W = M_\Sigma$ (for strangeness changing $\beta^-_{p\Delta S\pm1}$ and $\beta^-_{n\Delta S\pm1}$).

To calculated the discrete contribution for the $W = M$ we express the following functions used by Adler[4] in the notation of C.H. Llewellyn Smith [3] (which we use here).

$$|F_V(q^2)|^2 = |F_V^1(q^2)|^2 - \frac{q^2}{M^2}\left|\frac{\xi F_V^2(q^2)}{2}\right|^2$$

$$g_V(q^2) = F_V^1(q^2) + \xi F_V^2(q^2)$$

Note that $F_A(q^2)$ in our notation is the same as $g_A(q^2)$ as defined by Adler, and $F_P(q^2)$ in our notation is the same as $h_A(q^2)/M$ as defined by Adler. Also, Adler defines q^2 as positive, while we define q^2 as negative and Q^2 as positive.

If we separate out the discrete quasielastic delta function contributions, the two equations for the strangness-conserving ($\Delta S = 0$) Adler sum rules for β_p become:

$$|F_V(q^2)|^2 + [1/(cos^2\theta_c)] \ \ x$$

$$\int_{\nu_0}^\infty \left[W^{vec-}_{2p\Delta S=0}(\nu,q^2) - W^{vec+}_{2p\Delta S=0}(\nu,Q^2)\right] d\nu = 1$$

$$|F_A(q^2)|^2 + [1/(cos^2\theta_c)] \;\; x$$

$$\int_{\nu_0}^{\infty} \left[W^{ax-}_{2p\Delta S=0}(\nu, q^2) - W^{ax+}_{2p\Delta S=0}(\nu, Q^2) \right] d\nu = 1$$

Where the limits of the integrals are from pion threshold ν_0 where $W = M_\pi + M_P$ to $\nu_= \infty$.

The two equations for the strangness-conserving ($\Delta S = 0$) Adler sum rules for α_p become:

$$[1 + Q^2/4M^2][g_V(q^2)]^2 + [1/(cos^2\theta_c)] \;\; x$$

$$\int_{\nu_0}^{\infty} \left[W^{vec-}_{1p\Delta S=0}(\nu, q^2) - W^{vec+}_{1p\Delta S=0}(\nu, Q^2) \right] d\nu = C_{I,1}$$

$$[Q^2/4M^2][g_a(q^2)]^2 + [1/(cos^2\theta_c)] \;\; x$$

$$\int_{\nu_0}^{\infty} \left[W^{ax-}_{1p\Delta S=0}(\nu, q^2) - W^{ax+}_{1p\Delta S=0}(\nu, Q^2) \right] d\nu = C_{I,2}$$

Where the limits of the integrals are from pion threshold ν_0 where $W = M_\pi + M_P$ to $\nu_= \infty$.

The equationsfor the strangness-conserving ($\Delta S = 0$) Adler sum rule for γ_p become:

$$[g_a(q^2)][g_V(q^2)]/M = [1/(cos^2\theta_c)] \;\; x$$

$$\int_{\nu_0}^{\infty} \left[W^{-}_{3p\Delta S=0}(\nu, q^2) - W^{+}_{3p\Delta S=0}(\nu, Q^2) \right] d\nu$$

Where the limits of the integrals are from pion threshold ν_0 where $W = M_\pi + M_P$ to $\nu_= \infty$. Here $C_{I,1} = C_{I,2} = 1$ if simple quark-model commutation relations are valid. However, these may not be valid in theories in which meson fields are explicitly included in the currents. Therefore, testing the sum rule for W_1 is of interest (which requires a knowledge of the longitunidal structure function R).

The corresponding equations for α, β and γ for the strageness changing ($DeltaS \pm 1$) case for the proton and neutron are more complicated. The reader is refered to Adler's and Gilman's paper [4] for more details about current algebra sum rules for (α, β and γ) that could be tested for the first time with future precision electron scattering and neutrino scattering data. Note that these sum rules are expected to be valid over all values of Q^2. In addition to these neutrino sum rules, there are other sum rules based on dispersion relations that can be tested in electron scattering as described in Ref. [5]

22. Acknowledgements

This work is supported in part by the U. S. Department of Energy, High Energy Physics Division under grant DE-FG02-91ER40685 (Rochester). I thank H. Budd, G. Zeller, C. E. Keppel, D. Casper, J. Arrington, R. Ent and many others for significant contributions to this conference,

REFERENCES

1. Y. Fukada *et al.*, Phys. Rev. Lett. 81 (1998) 1562.
2. H. Budd, A. Bodek and J. Arrington, hep-ex/0308005 (published in Proceedings of NuInt02 - this conference, Nucl, Phys. B, Proceedings Suppl); A. Bodek, H. Budd and J. Arrington, hep-ex/0309024 (to be published in Proceedings of CIPANP2003, New York City, NY 2003.
3. C.H. Llewellyn Smith, Phys. Rep. 3C (1972).
4. S. Adler, Phys. Rev. **143**, 1144 (1966); F. Gillman, Phys. Rev. **167**, 1365 (1968).
5. D. Drechsel, B. Pasquini, M. Vanderhaeghen, hep-ph/0212123.
6. V. Bernard, L. Elouadrhiri, U.G. Meissner, J.Phys.G28 (2002), hep-ph/0107088.
7. J. Arrington, nucl-ex/0305009.
8. E. J. Brash*et al.*Phys., Rev. C, 65, 051001(R)
9. M. Paschos, private communication
10. M. Strikman, private communication
11. M. K. Jones *et al.*, Phys. Rev. Lett, 84, (2000) 1398 ; O. Gayou *et al.*, Phys. Rev. Lett, 88 (2002) 092301.
12. A.F. Krutov, V.E. Troitsky, Eur. Phys. J. A16 (2003) 285, hep-ph/0202183.
13. S. Glaster *et al.*, Nucl. Phys. B32 (1971) 221.
14. N.J. Baker *et al.*, Phys. Rev. D23 (1981) 2499.
15. S.J. Barish *et al.*, Phys. Rev. D16 (1977) 3103.
16. K.L. Miller *et al.*, Phys. Rev. D26 (1982) 537.
17. T. Kitagaki *et al.*, Phys. Rev. D26 (1983) 436.
18. T. Kitagaki *et al.*, Phys. Rev. Lett. 49 (1982) 98.
19. M.G. Olsson, E.T. Osyporeski and E.H. Monsay, Phys. Rev. D17 (1978) 2938.
20. S.K. Singh, Nucl. Phys. B36 (1972) 419.
21. Particle Data Group, Eur. Phys. J C15 (2000)

196.
22. W.A. Mann *et al.*, Phys. Rev. Lett. 31 (1973) 844.
23. J. Brunner *et al.*, Z. Phys. C45 (1990) 551.
24. M. Pohl *et al.*, Lett. Nuovo Cimento 26 (1979) 332.
25. L.B. Auerbach *et al.*, Phys. Rev. C66 (2002) 015501.
26. S.V. Belikov *et al.*, Z. Phys. A320 (1985) 625.
27. S. Bonetti *et al.*, Nuovo Cimento 38 (1977) 260.
28. N. Armenise *et al.*, Nucl. Phys. B152 (1979) 365.
29. G. Zeller, private communication.
30. R.A. Smith and E.J. Moniz, Nucl. Phys. B43 (1972) 605; E. J. Moniz *et al.*, Phys. Rev. Lett. 26. 445 (1971); E. J. Moniz, Phys. Rev. 184, 1154 (1969).
31. E. J. Moniz, private communication; W. Czyz and K. Gottfried, Nucl. Phys. **21**, 676 (1961); W. Czyz and K. Gottfried, Ann. Phys. NY **21**, 47 (1963);K. Gottfried, *ibid*, **21**, 29 (1963).
32. D. Casper, Nucl. Phys. Proc. Suppl. 112 (2002) 161.
33. K. Tsushima, Hungchong Kim, K. Saito, nucl-th[0307013].
34. A. Bodek and J. L. Ritchie, Phys. Rev. D23 (1981) 1070; ibid Phys. Rev. D24 (1981) 1400.
35. M. Strikman, private communication. See also talk by Rholf Ent, these proceedings; L. Lapikas, et al Phys.Rev.C61:064325,2000 (nucl-ex/9905009); L. Frankfurt, M. Strikman and M. Zhalov, Phys.Lett.B503:73-80,2001 (hep-ph/0011088)
36. Steve Manly (Rochester) and Will Brooks (Jlab) private communication.
37. See talks by Steve Manly (Rochester) and Jorge Morfin (this conference).
38. JLab hydrogen experiment 94-110, C.E. Keppel spokesperson
39. JLab deuterium experiment 02-109, C.E. Keppel, M. E. Christy, spokespersons
40. JLab experiment 99-118 on the nuclear dependence of R at low Q^2, A. Brull, C.E. Keppel spokespersons
41. Jlab Proposal PR03-110, A. Bodek and C. E. Keppel, Spokespersons;
42. U. K. Yang and A. Bodek, Phys. Rev. Lett. **82**, 2467 (1999).
43. U. K. Yang and A. Bodek, Eur. Phys. J. C**13**, 241 (2000).
44. U. K. Yang, Ph.D. thesis, Univ. of Rochester, UR-1583 (2001).
45. L. W. Whitlow *et al.* (SLAC-MIT) , Phys. Lett. B**282**, 433 (1995); A. C. Benvenuti *et al.* (BCDMS) , Phys. Lett. B**237**, 592 (1990); M. Arneodo *et al.* (NMC) , Nucl. Phys. B**483**, 3 (1997).
46. H. Georgi and H. D. Politzer, Phys. Rev. D**14**, 1829 (1976); R. Barbieri *et al.*, Phys. Lett. B**64**, 171 (1976), and Nucl. Phys. B**117**, 50 (1976); J. Pestieau and J. Urias, Phys.Rev.D**8**, 1552 (1973)
47. A.L. Kataev *et al.*, Phys. Lett. B**417**, 374 (1998), and also hep-ph/0106221; J. Bluemlein and A. Tkabladze, Nucl. Phys. B**553**, 427 (1999).
48. A. Bodek and U. K. Yang, `hep-ex/0203009`, (NuInt01 proceedings) Nucl.Phys.Proc.Suppl.112:70-76,2002.
49. A. Bodek, U. K. Yang, `hep-ex/0210024`, (NuFact'02 proceedings) J. Phys. G. Nucl. Part. Phys.,**29**, 1899 (2003); A. Bodek and U. K. Yang, `hep-ex/0308007`, (published in Proceedings of NuInt02 - this conference, Nucl, Phys. B, Proceedings Suppl); A. Bodek and U. K. Yang, `hep-ex/0301036` (proceedings of the Mexico Particle Physics summer school 2002).
50. A. Bodek *et al.*, Phys. Rev. D**20**, 1471 (1979).
51. A. Donnachie and P. V. Landshoff, Z. Phys. C **61**, 139 (1994); B. T. Fleming *et al.*(CCFR), Phys. Rev. Lett. **86**, 5430 (2001). Note that QCD evolution is completely neglected in these earlier analyses of very low Q^2 data. In contrast we include QCD evolution, low Q^2 non-perturbative effects target mass and higher twist terms in our fits.
52. S. Stein *et al.*, Phys. Rev. D**12**, 1884 (1975); K. Gottfried, Phys. Rev. Lett. **18**, 1174 (1967).
53. U. K. Yang *et al.*(CCFR), Phys. Rev. Lett. **87**, 251802 (2001).
54. E. D. Bloom and F. J. Gilman, Phys. Rev. Lett. **25**, 1140 (1970).

55. C. S. Armstrong *et al.*, Phys. Rev. D**63**, 094008 (2001) (www.jlab.org/resdata/). [also Phys. Rev. Lett. **85** , 1182 (2000); Phys. Rev. Lett. **85**, 1186 (2000); Phys. Rev. D **62**, 073008 (2000); Phys Rev. D **64**, 038302 (2001); Phys. Rev. C **64**, 014602 (2001); C. Keppel, Proc. of the Workshop on Exclusive Processes at High P_T, Newport News, VA, May (2002).]
56. D. Rein and L. M. Sehgal, Annals Phys. **133** 79 (1981) and D. Rein, Z. Phys. C. 35, 43 (1987) (neutrino production); R. P. Feynman, M. Kislinger, and F. Ravndal, Phys. Rev. D 3, 2706 (1971); FKR: F. Ravndal, Phys. Rev. D4, 1466 (1971) (electroproduction); Kneis, Moorhouse, Oberlack, Phys. Rev. D9, 2680 (1974) (photoproduction); R. Belusevic and D. Rein, Phys. Rev. D **46**, 3747 (1992) (neutrino coherent processes on nuclei).,
57. K. Sato and T. S. H. Lee nucl-th/0303050 (2003) (neutrino production); T. Sato, D. Uno and T.S. Lee, Phys. Rev. C63.-55201 (2001) (electroproduction)
58. S. Kretzer and M.H. Reno, hep-ph/0208187
59. Badelek and Kwiecinski, Nucl. Phys. **B370**, 278 (1992).